Nonlinear Dyn (2023) 111:9839–9861
https://doi.org/10.1007/s11071-023-08423-9

ORIGINAL PAPER

Inverted resonance capture cascade: modal interactions of a nonlinear energy sink with softening stiffness

Kevin Dekemele · **Giuseppe Habib**

Received: 14 December 2022 / Accepted: 16 March 2023 / Published online: 11 April 2023

Abstract Nonlinear energy sinks (NESs) are broadband passive vibration absorbers that are nonlinearly connected to a host system. If an NES is attached to a multi-degree-of-freedom mechanical host system under transient loading, the vibrations in the host system will transfer to and dissipate in the NES. During this transfer, the NES sequentially resonates with the modal frequencies of the host system, dissipating one mode at a time. This phenomenon is called resonance capture cascade (RCC). So far, RCC has only been investigated for NESs with a hardening nonlinear stiffness. Because of this stiffness, the transfer of modal vibrations happens from high to low frequency. In this study, an NES with a softening stiffness is proposed. Investigating the slow invariant manifolds reveals that an inverted resonance capture cascade occurs, where the transfer of vibrations to the NES is from low to high frequency. The analysis is carried out by exploiting high-dimensional slow invariant manifolds. The proposed NES is compared to the conventional NES with hardening stiffness.

Keywords Nonlinear energy sink · Resonance capture cascade · Nonlinear vibration absorber · Inverted resonance capture cascade

K. Dekemele
Department of Electromechanical, Systems and Metal Engineering, Ghent University, Tech Lane Ghent Science Park - Campus A, Technologiepark 125, B-9052 Ghent, Belgium
e-mail: kevin.dekemele@ugent.be

G. Habib
Department of Applied Mechanics, Faculty of Mechanical Engineering, Budapest University of Technology and Economics, Műegyetem rkp. 3., Budapest H-1111, Hungary

G. Habib (✉)
MTA-BME Lendület "Momentum" Global Dynamics Research Group, Budapest University of Technology and Economics, Műegyetem rkp. 3., Budapest H-1111, Hungary
e-mail: habib@mm.bme.hu

1 Introduction

Nonlinear energy sinks (NESs) are passive vibration absorbers, consisting of a small mass attached to the host system through a nonlinear spring and a damper [1–3]. Because of its nonlinear nature, the NES has a variable natural frequency, which increases its working bandwidth compared to conventional linear vibration absorbers, such as the tuned mass damper (TMD) [4]. Accordingly, in the case of broadband frequency vibrations, a small number of NESs can work more effectively than their linear counterpart, making the NES an attractive device in engineering.

Several types of NESs were proposed in the literature, apart from the classical one [3], which features a hardening polynomial stiffness. Examples are the vibro-impact NES [5–7], the rotating NES [8,9] and the bistable NES [10–12]. A common feature of these various devices is the broad frequency bandwidth of operation. The NES proved to be effective in various tasks, such as mitigation of transient [2,13,14], forced [15–18] and self-excited oscillations [19,20]; however,

some limitations about its effectiveness for suppressing limit cycle oscillations were also disclosed [21,22].

The NES is especially effective for suppressing vibrations of multi-degree-of-freedom (MDOF) mechanical systems with many vibration modes, each mode with its own shape and frequency [23]. Several studies illustrated that, under transient conditions, the NES mainly interacts with one vibration mode at a time. After dissipating most of the mechanical energy of one mode, the NES tunes to the subsequent mode, going from higher to lower frequency modes. This phenomenon is called resonance capture cascade (RCC) and is a consequence of the variable natural frequency property of the NES [2,24–27].

The RCC phenomenon was first discovered in 2003 [24] by investigating the nonlinear normal modes (NNMs) of the undamped system. Recently, in [28], the energy transfer duration per vibration mode was analytically estimated. The implemented procedure exploited the slow invariant manifold (SIM), which is the set of fixed points of oscillation amplitudes for the fast timescale. In [28], the SIM was limited to a two-dimensional space by assuming one active mode at the time. In [29], the SIM was extended to a multi-dimensional space by simultaneously considering all the vibration modes of the primary system activated. This approach provided a better understanding of the RCC based on the so-called interaction points. Considering that only one mode of the primary system is activated, the interaction points indicate the points of the SIM most affected by slight activation of other modes. They proved to be able to explain the RCC, providing a different point of view than its interpretation based on the NNMs. The RCC was experimentally obtained in [26,30].

Almost exclusively, all types of NES proposed in the literature present a hardening nonlinearity, in most cases cubic. The choice of a cubic restoring force is natural since it is probably the simplest and most studied type of nonlinearity (such as the Duffing oscillator [31]). Additionally, for any odd nonlinear function expanded in the Taylor series around the origin, a cubic term is the lowest-order nonlinear term, except for special cases. Furthermore, aiming at having a system with no linear component, the lowest order nonlinear term should be of hardening type to avoid a static instability in zero. Physical mechanisms utilized for generating nonlinear restoring force generally exploit geometrical nonlinearities, which usually can be reduced to hardening nonlinearities, in first approximation cubic. These involve transversely loaded strings [26,32], springs [33,34] or beams [35], magnets [36–38] or leafs springs [39]. Impact NES are one of the few types of NES whose restoring force is not reducible to a cubic term, but it is still of hardening type [5]. Between the few NES designs which are not strictly hardening, we mention the bistable NES [10,11], the pendulum NES [40], the periodically extended NES [41] and other non-smooth NESs [42] with descending stiffness [43]. Nevertheless, none of them has a strictly softening restoring force.

Recently, a mechanism that can generate a large range of stiffness characteristics was proposed and realized in practice [30,44,45]. The mechanism relies on a mass in contact with an arbitrarily shaped surface through a compressed linear spring, placed orthogonally with respect to the mass displacement. The shape of this force profile, which can be either machined or 3D-printed, determines the total stiffness characteristic. In particular, this mechanism can be used to generate a softening restoring force. Alternative methods for obtaining a softening restoring force function exist, such as topology optimization [46–48], magnetic forces [36,49] and metamaterials [48]. However, their effectiveness in real-world vibration control applications undergoing large vibrations is questionable since the displacement range for which the restoring force has a softening characteristic is usually limited [37].

Concerning the functionality of the NES, the possibility of freely choosing the restoring force function provides a significant advantage. In particular, the natural frequency of the conventional NESs (with hardening stiffness) increases with the NES's vibration amplitude. As such, the NES dissipates the higher frequency modes of the host system more efficiently than the lower frequency modes. Referring to the RCC, the NES tunes first with higher modes and then with lower ones. However, lower vibration modes typically contain more energy and cause larger displacements. Therefore, it would be beneficial to design an NES that dissipates first the lower frequency modes and does it more efficiently. With this objective, this paper investigates an NES with a softening stiffness, which has a natural frequency that decreases for increasing vibration amplitude. By exploiting high-dimensional SIMs, it will be shown that the modal interaction between an MDOF and a softening NES inverts the order in which the modal energy is transferred from the host system to the

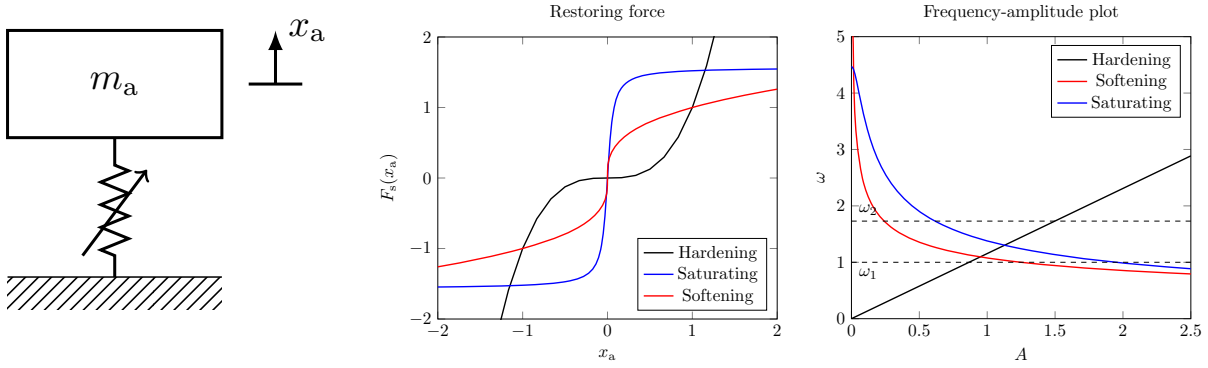

Fig. 1 **a** A simplified model of the nonlinear energy sink; **b** stiffness characteristics for hardening and softening stiffness; **c** relation between amplitude and natural frequency for the three different NESs considered

NES during RCC. This sequential transfer will now be from low- to high-frequency modes and, as such, the phenomenon will be called inverted resonance capture cascade (IRCC).

The paper is structured as follows: in Sect. 2, the frequency–amplitude relations of hardening and softening NESs are investigated. In the following section, the expressions and stability of higher-dimensional SIMs are derived. Then, the SIMs for a two-DOF primary system are discussed in Sect. 4 and compared to numerical simulations where one of the two modes are constant. Section 5 observes the (inverted) RCC for both the previously considered two-DOF system and a four-DOF system. Finally, the conclusions are presented.

2 Frequency–amplitude plot of an NES with softening stiffness

Figure 1a shows a generic undamped NES. The variable natural frequency of an NES can be illustrated by considering the unforced NES and applying harmonic balancing. This consists of an unforced single-DOF oscillator, whose dynamics is described by:

$$m_a\ddot{x}_a + f_{nl}(x_a) = 0. \tag{1}$$

Its steady-state solution is approximated by a Galerkin method, more precisely a projection on truncated Fourier series of a single harmonic [50,51], $x_a = A\sin(\omega T)$, where no assumption is made on ω. By then applying a standard harmonic balance technique [52] for frequency ω, Eq. (1) is transformed into:

$$\begin{aligned}
&\frac{\omega}{2\pi}\int_0^{\frac{2\pi}{\omega}} -m_a A\omega^2\sin^2(\omega T)dT \\
&\quad+\frac{\omega}{2\pi}\int_0^{\frac{2\pi}{\omega}} f_{nl}\left(A\sin(\omega T)\right)\sin\left(\omega T\right)dT = 0 \\
&\Rightarrow m_a A\omega^2\sin(\omega T) \\
&\quad-\frac{\omega}{2\pi}\int_0^{\frac{2\pi}{\omega}} f_{nl}\left(A\sin(\omega T)\right)\sin\left(\omega T\right)dT = 0
\end{aligned} \tag{2}$$

where the integral is the first harmonics from the truncated Fourier series. Three NESs are considered, which possess nonlinear restoring forces $f_{nl}(x_a)$ as depicted in Fig. 1b, namely one with a hardening stiffness x_a^3, one with a softening stiffness $\mathrm{sgn}(x_a)\sqrt[3]{|x_a|}$ and, finally, one with a softening but saturating stiffness $\arctan(20x_a)$. The relation between frequency and amplitude is found by solving the integral in Eq. (2), which yields:

$$\begin{aligned}
f_{nl}(x_a) = x_a^3 &: m_a\omega^2 = \frac{3A^2}{4} \\
f_{nl}(x_a) = \mathrm{sgn}(x_a)\sqrt[3]{|x_a|} &: m_a\omega^2 = \frac{3\Gamma\left(\frac{7}{6}\right)}{\sqrt{\pi}\Gamma\left(\frac{2}{3}\right)}\frac{1}{A^{\frac{2}{3}}} \\
f_{nl}(x_a) = \arctan(20x_a) &: m_a\omega^2 = 2\frac{\sqrt{400A^2+1}-1}{20A^2},
\end{aligned} \tag{3}$$

where $\Gamma(\cdot)$ is the Gamma function. The frequency–amplitude plots are shown in Fig. 1c, considering a unit mass. The natural frequency of the NES with hardening stiffness is linearly proportional to the vibration ampli-

tude, while it is inversely proportional for the NES with softening and saturating stiffness. For a hypothetical two-DOF host system, the natural frequencies are represented by dashed lines in Fig. 1c.

Generally speaking, the NES interacts with a natural frequency of the primary system when the line representing its natural frequency crosses the line of the natural frequency of the primary system. Consequently, the NES with hardening stiffness interacts with the higher mode of the primary system at a higher vibration amplitude than with the lower mode. The opposite holds for the NES with softening and saturating stiffness. This suggests that, assuming a sufficiently large energy content in the system, the NES with softening stiffness should dissipate the lower natural frequency earlier than the NES with hardening stiffness. Accordingly, the order of transfer of the vibration modes should also flip in the case of softening nonlinearity. This conjecture will be proved later on with a more rigorous approach.

The softening $\mathrm{sgn}(x_\mathrm{a})\sqrt[3]{|x_\mathrm{a}|}$, and softening and saturating $\arctan(20x_\mathrm{a})$ functions are similar both in characteristic and frequency–amplitude relation. However, when approaching zero amplitude, $\mathrm{sgn}(x_\mathrm{a})\sqrt[3]{|x_\mathrm{a}|}$'s derivative, and accordingly its frequency, goes to infinity, while $\arctan(20x_\mathrm{a})$'s derivative in zero is 20, i.e., its natural frequency tends to a constant value. Considering possible practical realizations of a softening NES, in [30,41,44] a device was presented that can tailor-make stiffness characteristics. It would not be able to achieve $\mathrm{sgn}(x_\mathrm{a})\sqrt[3]{|x_\mathrm{a}|}$ because of its infinity derivative; therefore, to facilitate computation and future experimental works, the softening and saturation arctan function will be used later on to showcase inverted resonance cascade, as its frequency–energy relation is very similar to the $\mathrm{sgn}(x_\mathrm{a})\sqrt[3]{|x_\mathrm{a}|}$ function. Furthermore, the algorithm used to generate the multi-dimensional SIMs can better deal with the finite derivative of the arctan function.

3 Slow invariant manifold for a generic primary system

Let us consider an n-DOF primary system with an attached NES, whose dynamics is modeled by the following system of differential equations

$$\sum_{j=1}^{n} m_{hj}\ddot{x}_j + \sum_{j=1}^{n} c_{hj}\dot{x}_j + \sum_{j=1}^{n} k_{hj}x_j = 0 \quad \text{for } h = 1, ..., n,\ h \neq l$$

$$\sum_{j=1}^{n} m_{lj}\ddot{x}_j + \sum_{j=1}^{n} c_{lj}\dot{x}_j + \sum_{j=1}^{n} k_{lj}x_j + \varepsilon(\ddot{x}_{n+1}) = 0$$

$$\varepsilon\ddot{x}_{n+1} + c_\mathrm{a}\left(\dot{x}_{n+1} - \dot{x}_l\right) + f_\mathrm{nl}\left(x_{n+1} - x_l\right) = 0, \quad (4)$$

where $m_{hj} = m_{jh}$, $c_{hj} = c_{jh}$ and $k_{hj} = k_{jh}$ are the terms of the primary system mass, damping and stiffness matrices, ε is the absorber mass, c_a is the absorber linear damping coefficient, x_1 to x_n are the primary system's coordinates and x_{n+1} the absorber's coordinate. ε is assumed small with respect to the primary system masses. Also, this study does not consider the special case of internal resonances. The absorber is assumed to directly interact only with the l^{th} DOF of the primary system.

To perform a modal analysis of the primary system, we temporarily neglect the contribution of the absorber, reducing the system to

$$\mathbf{M}\ddot{\mathbf{x}} + \mathbf{C}\dot{\mathbf{x}} + \mathbf{K}\mathbf{x} = \mathbf{0}, \quad (5)$$

where $\mathbf{M}$, $\mathbf{C}$ and $\mathbf{K}$ are $n \times n$ matrices (the full system has dimension $n+1$). We decouple the primary system by adopting the transformation $\mathbf{x} = \mathbf{U}\mathbf{q}$, where $\mathbf{U}$ contains the eigenvalues of $\mathbf{M}^{-1}\mathbf{K}$, normalized such that $\mathbf{U}^{\mathrm{T}}\mathbf{M}\mathbf{U} = \mathbf{I}$, where $\mathbf{I}$ is the identity matrix. $\mathbf{U}$ is defined as

$$\mathbf{U} = \begin{bmatrix} u_{11} & \cdots & u_{1n} \\ \vdots & \ddots & \vdots \\ u_{n1} & \cdots & u_{nn} \end{bmatrix}. \quad (6)$$

To simplify the notation, the damping matrix $\mathbf{C}$ is assumed given by a linear combination of $\mathbf{M}$ and $\mathbf{K}$, such that the primary system is fully decoupled in modal coordinates. This simplification does not affect the generality of the results. After the modal analysis, the primary system dynamics is described by the differential equations

$$\ddot{q}_h + 2\zeta_h\omega_h\dot{q}_h + \omega_h^2 q_h = 0 \quad \text{for } h = 1, ..., n, \quad (7)$$

where ω_h and ζ_h are the primary system's natural angular frequencies and modal damping ratios.

By considering the coordinate transformation and that the NES is attached to the l^{th} DOF of the primary system, we reintroduce the absorber into the system. We then obtain the system of differential equations

$$\ddot{q}_h + 2\zeta_h\omega_h\dot{q}_h + \omega_h^2 q_h = -u_{lh}\varepsilon\left(\ddot{z} - \sum_{j=1}^{n} u_{lj}\ddot{q}_j\right)$$
$$\text{for } h = 1, ..., n$$
$$\varepsilon\ddot{z} + c_a\dot{z} + f_{nl}(z) = \varepsilon\sum_{j=1}^{n} u_{lj}\ddot{q}_j, \tag{8}$$

where $z = x_l - x_{n+1}$. Next, we introduce the dimensionless damping parameter $\zeta_a = c_a/(2\varepsilon\omega_1)$, attaining

$$\ddot{q}_h + 2\zeta_h\omega_h\dot{q}_h + \omega_h^2 q_h = -u_{lh}\varepsilon\left(\ddot{z} - \sum_{j=1}^{n} u_{lj}\ddot{q}_j\right)$$
$$\text{for } h = 1, ..., n$$
$$\ddot{z} + 2\zeta_a\omega_1\dot{z} + \frac{f_{nl}(z)}{\varepsilon} = \sum_{j=1}^{n} u_{lj}\ddot{q}_j. \tag{9}$$

3.1 Slow invariant manifold and stability

Aiming at characterizing the behavior of the NES against impulsive excitations, we seek the SIM describing the slow dynamics of the system. Considering typical practical constraints, we assume that ε is a small parameter ($\varepsilon \ll 1$). To obtain the SIM, the dynamic variables are substituted by the complex variables of Manevitch $A_h(T), B_j(T) \in \mathbb{C}$ [53]:

$$\begin{aligned} 2A_h(T)e^{i\omega_h T} &= q_h - i\dot{q}_h/\omega_h \\ 2B_j(T)e^{i\omega_j T} &= z_j - i\dot{z}_j/\omega_j \end{aligned} \tag{10}$$

where the original variables are then substituted by:

$$\begin{aligned} q_h &= A_h(T)e^{i\omega_h T} + A_h^*(T)e^{-i\omega_h T} \\ \dot{q}_h &= i\omega_h A_h(T)e^{i\omega_h T} - i\omega_h A_h^*(T)e^{-i\omega_h T} \\ &\text{for } h = 1, ..., n \end{aligned} \tag{11}$$

$$z \approx \sum_{j=1}^{n} \underbrace{B_j(T)e^{i\omega_j T} + B_j^*(T)e^{-i\omega_j T}}_{z_j}$$
$$\dot{z} \approx \sum_{j=1}^{n} \underbrace{i\omega_j B_j(T)e^{i\omega_j T} - i\omega_j B_j^*(T)e^{-i\omega_j T}}_{\dot{z}_j} \tag{12}$$

where * stands for complex conjugate and z_j is the contribution of mode j to z.

Deriving (10) w.r.t. time yields, after some steps [41]:

$$\begin{aligned} \ddot{q}_h + \omega_h^2 q_h &= i2\omega_h\dot{A}_h e^{i\omega_h T} \\ \ddot{z}_j + \omega_j^2 z_j &= i2\omega_j\dot{B}_j e^{i\omega_j T}. \end{aligned} \tag{13}$$

The total relative acceleration of the NES is $\ddot{z} = \sum_{j=1}^{n}\ddot{z}_j$. Substituting (11), (12) and (13) into (9) and applying harmonic balancing (keeping only terms of $e^{i\omega_h T}$) yield:

$$\begin{aligned} &2\omega_h\dot{A}_h + 2\zeta_h\omega_h^2 A_h = \\ &\quad -u_{lh}\varepsilon(2\omega_h\dot{B}_h - i\omega_h^2 B_h - 2u_{lh}\omega_h\dot{A}_h + iu_{lh}\omega_h^2 A_h) \\ &2\omega_h\dot{B}_h - i\omega_h^2 B_h + 2\zeta_a\omega_1\omega_h B_h \\ &\quad + iB_h G_h(|B_1|, ..., |B_n|) = u_{lh}\left(2\omega_h\dot{A}_h - i\omega_h^2 A_h\right) \\ &\quad \text{for } h = 1, ..., n, \end{aligned} \tag{14}$$

where the term $B_h G_h(|B_1|, ..., |B_n|)$ in (14) is the Fourier coefficient for ω_h of the multidimensional Fourier series. A multidimensional harmonic balancing method [52,54,55] is applied, which can deal with multi- and quasi-periodic vibrations. The first step is to separate the vibrations into distinct time variables:

$$T_j = \omega_j T \quad \text{for } j = 1, ..., n \tag{15}$$

The multidimensional Fourier coefficient for ω_h then is

$$\begin{aligned} &B_h(2\pi)^n\varepsilon G_h \\ &= \int_0^{2\pi}\cdots\int_0^{2\pi} f_{nl}\left(\sum_{j=1}^{n} B_j e^{iT_j} + B_j^* e^{-iT_j}\right) \\ &\quad \times e^{iT_h} dT_1 \ldots dT_n. \end{aligned} \tag{16}$$

The integral (16) is generally hard to solve analytically, except if the restoring force is assumed to have the following form:

$$f_{nl} \approx k_a\left(x_{n+1} - x_l\right) + \sum_{r=1}^{g} k_{a2r+1}\left(x_{n+1} - x_l\right)^{2r+1}. \tag{17}$$

The summation $\sum_{r=1}^{g} k_{a2r+1}\left(x_{n+1} - x_l\right)^{2r+1}$ indicates a generic polynomial series representation of the

restoring force of the NES—which is assumed odd—excluding the linear term, and where $2g+1$ is the highest polynomial order considered. This series can be an exact representation of the restoring force but can also be obtained from Taylor's series expansion or least-squared fitting of the stiffness characteristic over a certain range. The polynomial series allows for an analytical expression under harmonic balancing [29] for the quasi-periodic vibrations of the NES, as the natural frequencies of the primary system are assumed incommensurate and remote. For now, no assumption will be made on f_{nl} to keep the generic nature of the equations, but Eq. (17) will be applied in the numerical examples further on.

Then, the dynamics in (14) are split into two time scales, a fast time τ_0 and a slow time τ_1:

$$\begin{aligned} &A_h(T) = A_h(\tau_0,\tau_1) \quad B_h(T) = B_h(\tau_0,\tau_1) \\ &\tau_0 = T,\ \tau_1 = \varepsilon T \quad \frac{d}{dT} = \frac{\partial}{\partial\tau_0} + \varepsilon\frac{\partial}{\partial\tau_1} \end{aligned} \tag{18}$$

By applying this procedure to (14) and collecting terms according to their order in ε, we attain

$$\begin{aligned} &\frac{\partial A_h}{\partial\tau_0} = 0 \\ &2\omega_h\frac{\partial A_h}{\partial\tau_1} + 2\xi_h\omega_h^2 A_h \\ &\quad = -u_{lh}\left(2\omega_h\frac{\partial B_h}{\partial\tau_0}\right. \\ &\quad \left. -i\omega_h^2 B_h - 2u_{lh}\omega_h\frac{\partial A_h}{\partial\tau_0} + iu_{lh}\omega_h^2 A_h\right) \\ &2\omega_h\frac{\partial B_h}{\partial\tau_0} - i\omega_h^2 B_h + 2\zeta_a\omega_1\omega_h B_h \\ &\quad + iB_h G_h(|B_1|,...,|B_n|) \\ &\quad = u_{lh}\left(2\omega_h\frac{\partial A_h}{\partial\tau_0} - i\omega_h^2 A_h\right) \\ &\text{for } h = 1,...,n, \end{aligned} \tag{19}$$

where $\xi_h = \zeta_h/\varepsilon$. To obtain the slow flow dynamics from Eq. (19), the (fast) time derivatives with respect to τ_0 will be assumed zero, leading to a steady-state solution in this time scale. An $n+1$-dimensional slow invariant manifold that governs the relation between A_h and B_j, for $j = 1,...,n$ will be found. To verify the assumption that a steady-state motion exists, the stability in τ_0 will be obtained from Eq. (19) as well.

3.1.1 Slow invariant manifold

In the second and third equations of (19), derivatives of B_h with respect to τ are set to zero, and A_h and B_h are defined as $A_h = a_h e^{i\alpha_h}/2$ and $B_h = b_h e^{i\beta_h}/2$. Then, the equations are split into their real and imaginary parts, yielding the following equations:

$$\begin{aligned} &2\frac{\partial a_h}{\partial\tau_1} = -2\xi_h\omega_h a_h + u_{lh}\omega_h b_h\sin(\beta_h-\alpha_h) \\ &2a_h\frac{\partial\alpha_h}{\partial\tau_1} = -u_{lh}\left(-\omega_h b_h\cos(\beta_h-\alpha_h) + u_{lh}\omega_h a_h\right) \\ &2\zeta_a\omega_1\omega_h b_h = u_{lh}\omega_h^2 a_h\sin(\beta_h-\alpha_h) \\ &\quad -\omega_h^2 b_h + b_h G_h(b_1,...,b_n) \\ &\quad = u_{lh}\omega_h^2 a_h\cos(\beta_h-\alpha_h) \\ &\quad \text{for } h = 1,...,n. \end{aligned} \tag{20}$$

Subsequently, inserting the third into the first equations of (20), and squaring and adding the third and fourth equations yield the slow flow dynamics and slow invariant manifold, i.e.,

$$\begin{aligned} &\frac{\partial a_h^2}{\partial\tau_1} = -2\xi_h\omega_h a_h^2 - 2\zeta_a\omega_1 b_h^2 \\ &u_{lh}^2\omega_h^4 a_h^2 = b_h^2\left(\left(\omega_h^2 - G_h(b_1,...,b_n)\right)^2 + 4\zeta_a^2\omega_1^2\omega_h^2\right) \\ &\quad \text{for } h = 1,...,n. \end{aligned} \tag{21}$$

These form a system of differential equations and one of algebraic equations defining the SIM of the system. a_h indicates the amplitude of oscillation of the h^{th} mode of the primary system, while b_h indicates the component of the relative amplitude of oscillation of the absorber at ω_h angular frequency. The differential equations of (21) imply that a_h will decrease if there is damping in the NES or modal damping in the primary system. The algebraic equations define the SIM that confines the relation between the modal amplitudes of the host system $(a_1,...,a_n)$ and of the NES $(b_1,...,b_n)$.

3.1.2 Stability

In order to obtain the SIM and slow flow dynamics, it was assumed that derivatives of B_h with respect to τ_0 were zero. To verify this assumption, the stability of B_h in τ_0 is determined by linearizing the last set of equations of (19) around the fixed points on the SIM obtained from (21), and determining the eigenvalues

of the Jacobian matrix. As $\partial A_h/\partial \tau_0 = 0$, A_h is not perturbed in this procedure. This procedure is common to determine the stability of SIMs [34,41]. We obtain from the linearization

$$\begin{bmatrix} \frac{\partial \Delta \mathbf{B}}{\partial \tau_0} \\ \frac{\partial \Delta \mathbf{B}^*}{\partial \tau_0} \end{bmatrix} = \underbrace{\begin{bmatrix} \frac{\partial \mathbf{f}}{\partial \mathbf{B}} & \frac{\partial \mathbf{f}}{\partial \mathbf{B}^*} \\ \frac{\partial \mathbf{f}^*}{\partial \mathbf{B}} & \frac{\partial \mathbf{f}^*}{\partial \mathbf{B}^*} \end{bmatrix}}_{\mathbf{J}} \begin{bmatrix} \Delta \mathbf{B} \\ \Delta \mathbf{B}^* \end{bmatrix}, \tag{22}$$

where * stand for complex conjugate, $\Delta \mathbf{B} = [\Delta B_1, ..., \Delta B_n]^T$, $\Delta B_h = B_h - B_{h,\mathrm{eq}}$, $B_{h,\mathrm{eq}}$ is the value of B_h in the fixed point, and $\mathbf{J}$ is the Jacobian. If the Jacobian has any eigenvalue with a positive real part, the fixed point is unstable. The Jacobian's submatrices are defined as:

$$\begin{aligned} \frac{\partial \mathbf{f}}{\partial \mathbf{B}} &= \begin{bmatrix} \frac{\partial f_1}{\partial B_1} & \cdots & \frac{\partial f_1}{\partial B_n} \\ \vdots & \ddots & \vdots \\ \frac{\partial f_n}{\partial B_1} & \cdots & \frac{\partial f_n}{\partial B_n} \end{bmatrix} \quad \frac{\partial \mathbf{f}}{\partial \mathbf{B}^*} = \begin{bmatrix} \frac{\partial f_1}{\partial B_1^*} & \cdots & \frac{\partial f_1}{\partial B_n^*} \\ \vdots & \ddots & \vdots \\ \frac{\partial f_n}{\partial B_1^*} & \cdots & \frac{\partial f_n}{\partial B_n^*} \end{bmatrix} \\ \frac{\partial \mathbf{f}^*}{\partial \mathbf{B}} &= \left(\frac{\partial \mathbf{f}}{\partial \mathbf{B}^*}\right)^* \quad \frac{\partial \mathbf{f}^*}{\partial \mathbf{B}^*} = \left(\frac{\partial \mathbf{f}}{\partial \mathbf{B}}\right)^* \end{aligned} \tag{23}$$

where f_h is a recollected version of the final equation of (19):

$$\begin{aligned} f_h = \frac{1}{2\omega_h}\big(& - u_{lh} i \omega_h^2 A_h + i \omega_h^2 B_h - 2\zeta_\mathrm{a} \omega_1 \omega_h \\ & - i B_h G_h(|B_1|, ..., |B_n|)\big) \\ & \text{for } h = 1, ..., n. \end{aligned} \tag{24}$$

3.1.3 Interaction points

The SIM presented in Eq. (21) is very informative regarding the system's slow dynamics since it can characterize the mutual effect of each modal vibration of the primary system on the NES. However, it is quite complex to visualize it because it exists in a $2n$-dimensional space. In most studies about the SIM of NES, the SIM is limited to a single mode, which reduces it to a curve in a two-dimensional space. Indeed, this representation constitutes a good starting point for studying the effect of other modes on the one under study. With this purpose, in [29], the so-called *interaction points* were defined. Their meaning and implications are explained below.

Let us consider that only one mode of the primary system, a_h, is activated. In this case, only $b_h \neq 0$, while $b_j = 0$ for any $j \neq h$. The SIM is then reduced to a line in the two-dimensional space a_h, b_h. If any of the other modes a_j is activated ($a_j \neq 0$, but small), then the SIM in the a_h, b_h will be affected, but only in a specific region around a point called interaction point b_h-b_j.

The interaction point b_h-b_j can be found by considering the j^{th} equation of (21), and assuming that $b_h \gg b_i$ for $i \neq h$ (therefore including $i = j$). For illustration, we consider the example of a hardening and a softening stiffness, both locally approximated by a third-order polynomial (see Eq. (17)), such that $G_h = \omega_\mathrm{a}^2 + \gamma_3 \left(3b_h^2 + 6b_j^2\right)/4$, with $\omega_\mathrm{a} = \sqrt{k_{\mathrm{a}1}/\varepsilon}$, where $\gamma_3 > 0$ for a hardening stiffness and $\gamma_3 < 0$ for a softening stiffness.

This assumption reduces the jth equation of (21) to

$$b_j^2 = \frac{u_{lj}^2 \omega_j^4 a_j^2}{\left(\omega_j^2 - \omega_\mathrm{a}^2 - \gamma_3 \frac{3}{2} b_h^2\right)^2 + 4\zeta_\mathrm{a}^2 \omega_1^2 \omega_j^2}. \tag{25}$$

Equation (25) has a maximum for

$$b_h^2 = \frac{2\left(\omega_j^2 - \omega_\mathrm{a}^2\right)}{3\gamma_3}. \tag{26}$$

Since this value corresponds to the point where b_j is maximal, it is also the point where it has the largest effect on b_h. By substituting Eq. (26) into the hth Eq. (21), we obtain

$$a_h^2 = \frac{2\left(\omega_j^2 - \omega_\mathrm{a}^2\right)}{3\gamma_3 u_{lh}^2 \omega_h^4} \left(\left(\omega_h^2 - \frac{\omega_\mathrm{a}^2 + \omega_j^2}{2}\right)^2 + 4\zeta_\mathrm{a}^2 \omega_1^2 \omega_h^2\right). \tag{27}$$

Equations (27) and (26) explicitly identify the interaction point b_h-b_j in the a_h, b_h space. If different polynomial orders are considered in the NES restoring force, the equations are not valid anymore, but the same procedure can be adopted.

We note that, for the case of a hardening NES ($\gamma_3 > 0$), a resonant point exists only if $\omega_j > \omega_\mathrm{a}$. Conversely, for a softening NES ($\gamma_3 < 0$), it exists only if $\omega_j < \omega_\mathrm{a}$. This observation is consistent with the fact

that the NES can resonate with one mode only if the frequency backbone passes through its natural frequency. Therefore, if the mode has a natural frequency ω_j larger than the linear natural frequency of the NES ω_a, only in the case of hardening NES the frequency backbone of the NES can reach ω_j. The opposite is valid for a softening NES. This implies that, for a hardening NES, ω_a should be smaller or equal to the smallest natural frequency of the primary system ($\omega_a \leq \omega_1$). Contrariwise, for a softening NES, ω_a should be larger than the largest natural frequency of the primary system ($\omega_a \geq \omega_n$). In general, hardening NESs have $\omega_a = 0$.

Although the passages just presented do not demonstrate the existence of the interaction points, a numerical example presented in [29] illustrates their practical relevance for the case of a purely cubic NES. In the following of this work, they will be utilized to study the mutual effect of the amplitude of oscillation of different modes on the NES and to present the inverted RCC.

4 Study for a two-DOF host system

4.1 System description

An undamped two-DOF chain of masses, with identical masses and stiffnesses, is considered as a host system, as illustrated in Fig. 2. The equations of motion with an NES attached to the second mass read:

$$\begin{aligned} &m\ddot{x}_1 + 2kx_1 - kx_2 = 0 \\ &m\ddot{x}_2 - kx_1 + 2kx_2 + \varepsilon\ddot{x}_3 = 0 \\ &\varepsilon\ddot{x}_3 + c_a\left(\dot{x}_3 - \dot{x}_2\right) + f_{\mathrm{nl}}(x_3 - x_2) = 0 \end{aligned} \tag{28}$$

where, without loss of generality, we assume all dimensionless quantities, besides $m = 1$, $k = 1$, $\varepsilon = 0.02$ and $\zeta_a = 0.05$ (these numerical values are used throughout the whole study); $f_{\mathrm{nl}}(z)$ is the absorber's restoring force. The natural frequencies are $\omega_1 = 1$ and $\omega_2 = \sqrt{3}$, which exclude internal resonances. The modal mass normalized eigenvectors at the location of the second mass are $u_{21} = \sqrt{2}/2$ and $u_{22} = -\sqrt{2}/2$. A hardening and a softening restoring force will be compared, namely

$$\begin{aligned} &\text{Hardening:} \quad f_{\mathrm{nl}}(z) = \varepsilon z^3 \\ &\text{Softening:} \quad f_{\mathrm{nl}}(z) = \varepsilon \arctan(20z). \end{aligned} \tag{29}$$

In modal coordinates, the equations of motion are:

$$\begin{aligned} &\ddot{q}_1 + 2\zeta_1\omega_1\dot{q}_1 + \omega_1^2 q_1 = u_{21}\varepsilon\left(2\zeta_a\omega_1\dot{z} + \frac{f_{\mathrm{nl}}(z)}{\varepsilon}\right) \\ &\ddot{q}_2 + 2\zeta_h\omega_2\dot{q}_h + \omega_2^2 q_h = u_{22}\varepsilon\left(2\zeta_a\omega_1\dot{z} + \frac{f_{\mathrm{nl}}(z)}{\varepsilon}\right) \\ &\text{Hardening}: \ddot{z} + 2\zeta_a\omega_1\dot{z} + z^3 = \sum_{j=1}^{n} u_{lj}\ddot{q}_j \\ &\text{Softening}: \ddot{z} + 2\zeta_a\omega_1\dot{z} + \arctan(20z) = \sum_{j=1}^{n} u_{lj}\ddot{q}_j. \end{aligned} \tag{30}$$

4.2 Slow invariant manifold

The SIM for the hardening NES, where $n = l = 2$ and $\gamma_3 = 1$, is described by

$$\begin{aligned} u_{21}^2\omega_1^4 a_1^2 &= b_1^2\left(\left(\omega_1^2 - \frac{\gamma_3}{4}\left(3b_1^2 + 6b_2^2\right)\right)^2 + 4\zeta_a^2\omega_1^4\right) \\ u_{22}^2\omega_2^4 a_2^2 &= b_2^2\left(\left(\omega_2^2 - \frac{\gamma_3}{4}\left(3b_2^2 + 6b_1^2\right)\right)^2 + 4\zeta_a^2\omega_1^2\omega_2^2\right), \end{aligned} \tag{31}$$

while the SIM for the softening NES is given by

$$\begin{aligned} u_{21}^2\omega_1^4 a_1^2 &= b_1^2\left(\left(\omega_1^2 - G_1(b_1, b_2)\right)^2 + 4\zeta_a^2\omega_1^4\right) \\ u_{22}^2\omega_2^4 a_2^2 &= b_2^2\left(\left(\omega_2^2 - G_2(b_1, b_2)\right)^2 + 4\zeta_a^2\omega_1^2\omega_2^2\right). \end{aligned} \tag{32}$$

G_1 and G_2 can be obtained from solving the integral (16); however, an analytical solution to that inte-

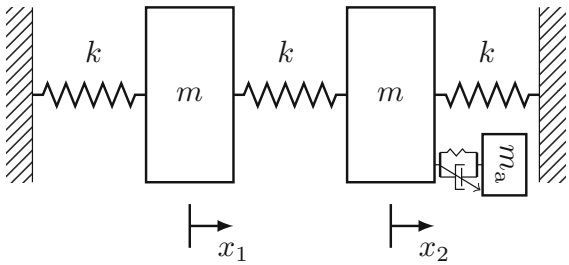

Fig. 2 Two-DOF mechanical host system with an NES connected to the second mass

gral cannot be obtained with standard techniques while numerically computing this integral is very slow. Therefore, for plotting the manifold and studying its stability, the integral is solved semi-analytically by exploiting a polynomial least square approximation. This approximation allows for a fast and converging continuation and stability computation of (32), similarly as in [29].

In the special case where there is only a single active mode, we have $a_h \neq 0$, $b_h \neq 0$, $a_j = b_j = 0$ where $j \neq h$. Accordingly, an exact analytical expression for $G_h(b_h)$ for the softening NES is found directly through harmonic balancing without resorting to a refitting of polynomial series. Solving the single integral (16) for that case:

$$\begin{aligned} G_h(b_h) &= \frac{1}{2\pi B_h} \int_0^{2\pi} \\ &\quad \times \arctan\left(20\left(B_h e^{iT_h} + B_h^* e^{-iT_h}\right)\right) e^{-iT_h} dT_h \\ &= \frac{\sqrt{400b_h^2 + 1} - 1}{10b_h^2} \end{aligned} \tag{33}$$

4.3 SIMs with no activated other modes

The case where only a single mode is active for a hardening NES has been extensively studied in the literature [11,28–30,33,41,56,57]. The curves in Fig. 3a–b and c–d depict the SIMs for the hardening and softening stiffness, respectively. All SIMs have the same topology: three branches, of which the dashed middle one is unstable, separated by two folds. The left stable branch is suboptimal, as for this branch, the absorber relative displacement (b_h) is low; consequently, the decay will be slow, as indicated by the first equation of (21). (We remind that the host system damping is neglected, and the absorber relative velocity is the only source of energy dissipation.) The right branch has high absorber activity and, as such, enables fast energy decay. If the dynamics start on the right branch, the NES engages in efficient targeted energy transfer (TET). It was established in [28,33,57] that, to ensure TET, the initial energy of the primary system should be above the fold in the local maximum. For energy levels between the two folds, the TET triggering depends on the system's initial conditions.

4.4 SIMs with slightly activated other mode and interaction points

Let us now consider the case of one mode of the primary system strongly activated and the other one only slightly.

4.4.1 Hardening stiffness

The SIMs for the hardening stiffness are shown in Fig. 4. To reduce the dimensionality of the problem (see Eq. (21)), Fig. 4a and b is obtained by assuming a constant a_2, which allows 2-dimensional projections of the SIM. For $a_2 = 0.01$, the projection of the SIM in the a_1, b_1 space (Fig. 4a) exhibits the typical 3-branch curve with two folds, the stable left and right branch, and the unstable middle branch. It is practically identical to the SIM for a single activated mode in Fig. 3a.

By slightly increasing the primary system's second vibration mode's amplitude a_2, a tongue appears on the right branch of the SIM, which is the branch with the best dissipation performance. The tongue bends to the left for increasing a_2, decreasing b_1 for constant a_1; the practical effect of this phenomenon is a reduction in the dissipation rate, which is proportional to b_1. Thus, even a small amount of a_2 will decrease the performance of the NES in dissipating a_1. As expected, the tongue's onset is on the interaction point b_1-b_2, marked by a blue dot in Fig. 4a. To clarify this aspect, we note that the interaction point has coordinate $a_1 = 1.02$—as identified through Eq. (27)—that is the value of a_1 for which b_2 is maximal. This is illustrated by the curve in Fig. 4b, which resembles a resonance curve. From a purely analytic perspective, this means that b_2 cannot be neglected in the first equation of (31). In practice, it means that energy of the host system's second mode is pumped into the NES. As a_2 increases, the peak in Fig. 4b, moves to the right, i.e., to higher a_1 values; accordingly, the tongue in Fig. 4a moves upwards, also to higher a_1 values.

The effect on a_2 of small, but not negligible, a_1 values is now studied through Fig. 4c and d, which are analogous to Figs. 4a and b, respectively, with the difference that now the second mode of the primary system is the one fully activated ($a_2 \neq 0$), while a_1 is small. Referring to the SIM in Fig. 4c for $a_1 = 0.01$, we note that now the interaction point b_2-b_1 is on the left branch, i.e., the branch with worse dissipation performance. The position of the interaction point sug-

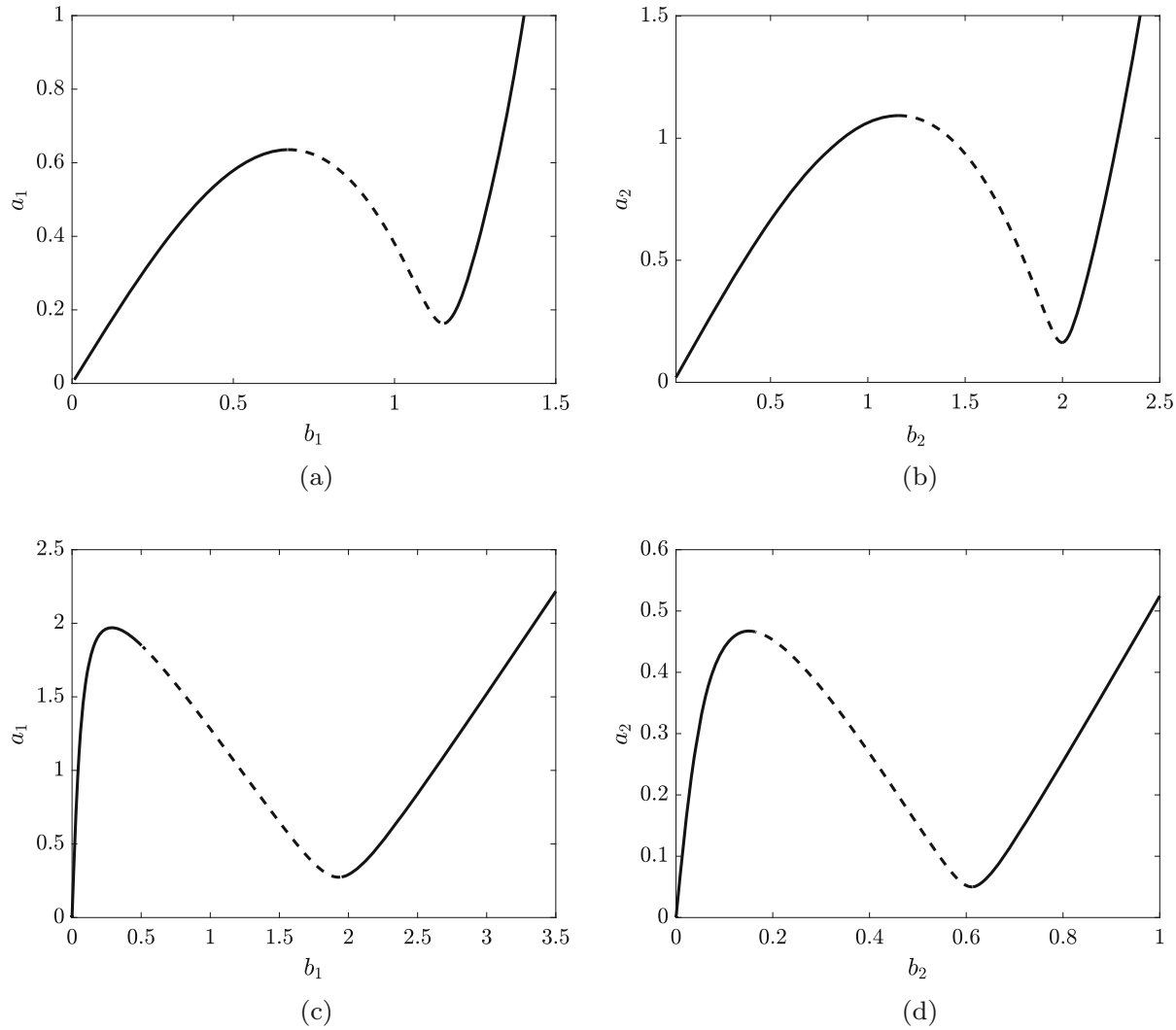

Fig. 3 SIMs for the system in Eq. (30), assuming energy on a single mode of the primary system. **a** and **b** refer to the hardening case, **c** and **d** to the softening one; dashed lines indicate unstable solutions

gests that increasing a_1 will have a major effect on the left branch, which is less relevant concerning the absorber's performance. This observation is fully confirmed by increasing a_1; in fact, also this time, a tongue is generated in the vicinity of the interaction point, as expected. Additionally, even a small value of a_1 lowers the left branch, and the branch becomes rapidly unstable (for $a_1 = 0.15$); accordingly, the required threshold $a_2(0)$ to jump to the right branch and engage in TET decreases. In other words, a small a_1 value improves the ability of the absorber to dissipate vibrations in the second mode. Regarding the relation between a_2 and b_1 illustrated in Fig. 4d, the peak of the curve now bends to lower a_2 values for increasing a_1, differently from the previous case, illustrated in Fig. 4b.

Thus, for hardening stiffness, a small amount of a_2 (higher frequency mode) decreases the NES performance for a_1 (lower frequency mode). Conversely, a small amount of a_1 (lower frequency mode) increases the NES performance for a_2. Later on, when the modes are both activated significantly, this will cause the resonance capture cascade effect, where the presence of a large amount of energy on the primary system's second mode (large a_2) will drastically reduce b_1, and thus the dissipation of a_1, while the presence of a large amount of energy on the primary system's first mode (large a_1)

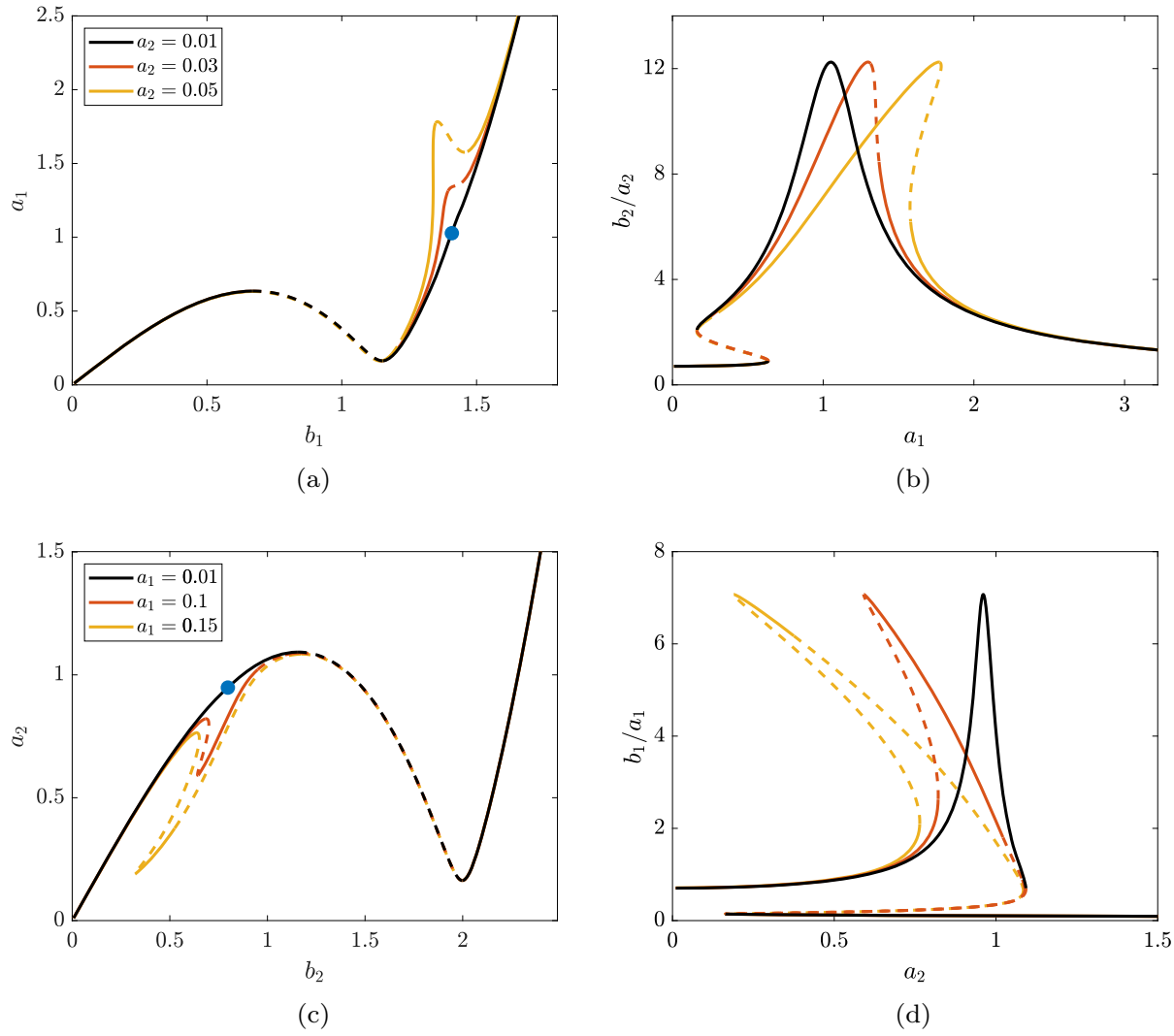

Fig. 4 Sections of the SIM for a hardening NES, to study the effect of slightly activated modes. **a** $a_1 - b_1$ SIM section for several constant a_2; **b** the corresponding $b_2/a_2 - a_1$ curve; **c** $a_2 - b_2$ SIM section for several constant a_1; **d** the corresponding $b_1/a_1 - a_2$ curve

will force a_2 to dissipate quickly. Only after a_2 is dissipated and sufficiently low, the efficient right branch of the SIM in the a_1, b_1 space is reinstated, and a_1 is dissipated efficiently. This phenomenon explains the sequence from high-to-low modal dissipation by the NES, as thoroughly discussed in [29].

4.4.2 Softening stiffness

The SIMs for the softening stiffness case are depicted in Fig. 5. Comparing Fig. 5 with Fig. 4, we note different positions of the interaction points. In Fig. 5a and c, the interaction points are on the left and on the right branch, respectively, while in Fig. 4a and c they were positioned oppositely. This observation suggests that, for a softening nonlinearity, a small a_2 value will improve energy dissipation on the first mode, while a small amount of energy on the first mode of the primary system (a_1) will reduce energy dissipation of the second mode, exactly the opposite of what occurs in the hardening case. This scenario is confirmed by the tongues illustrated in Fig. 5a and c. In both cases, the

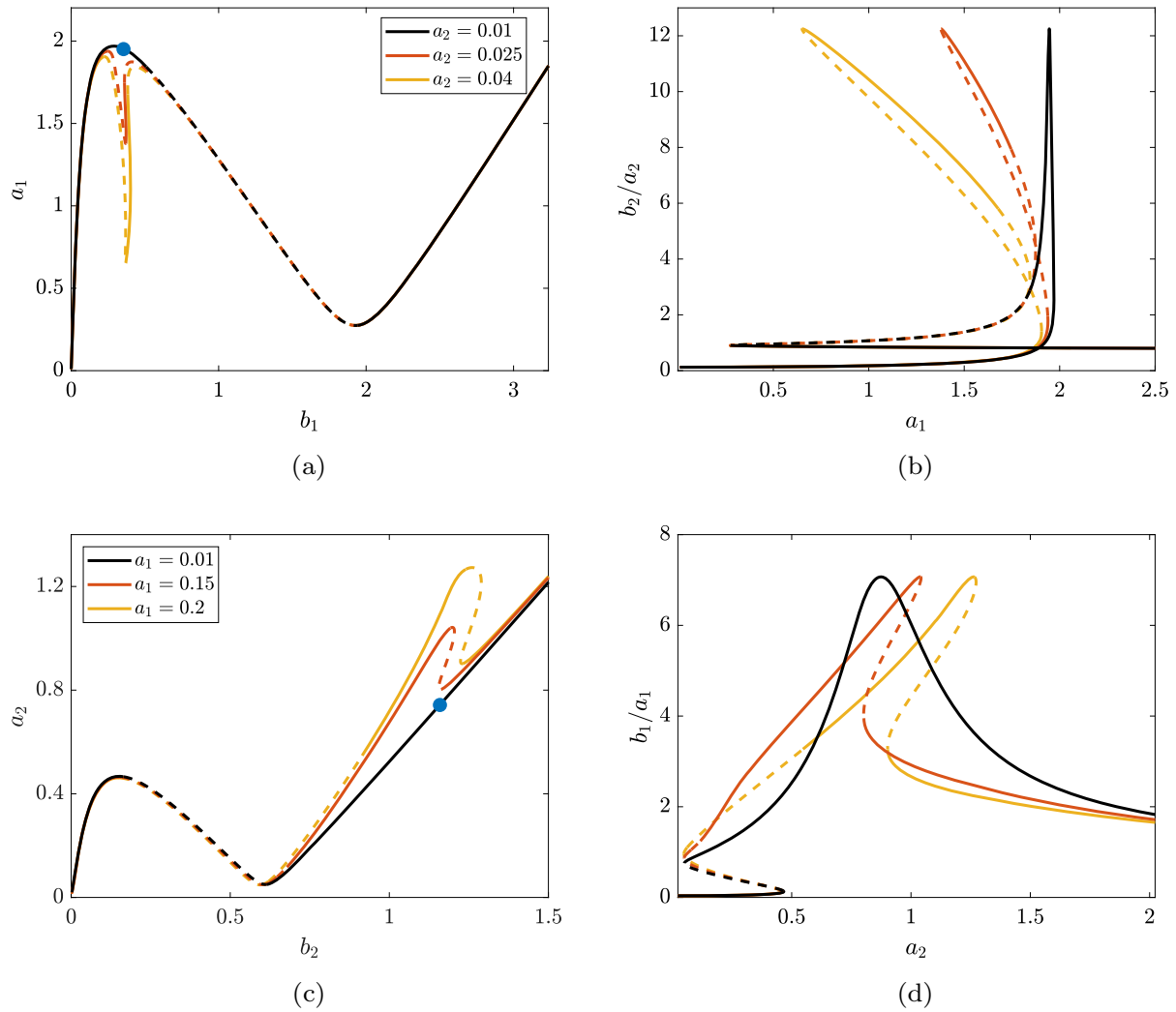

Fig. 5 Sections of the SIM for a softening NES, to study the effect of slightly activated modes. **a** $a_1 - b_1$ SIM section for several constant a_2; **b** the corresponding $b_2/a_2 - a_1$ curve; **c** $a_2 - b_2$ SIM section for several constant a_1; **d** the corresponding $b_1/a_1 - a_2$ curve

tongues are generated in correspondence with the interaction points. The same argumentation presented for the hardening case is valid also for the softening case but in an opposite way. In Fig. 5b and d, the trend of the NES amplitude for the slightly activated mode (respectively, b_2 and b_1) is illustrated. The peak moves to the left when the slightly activated mode is the higher one, and to the right in the other case. The opposite was observed for the hardening case.

According to these observations regarding the SIM evolution for softening stiffness, a small amount of a_2 (higher frequency mode) will increase the NES performance for a_1 (lower frequency mode). Conversely, a small amount of a_1 (lower frequency mode) will decrease the NES performance for a_2 (higher frequency mode). Later, it will be shown that these modal interactions are the mechanism behind the inverted resonance capture cascade when both modes are significantly activated.

4.5 SIMs with strongly activated other modes

4.5.1 Effect on SIM

In Sect. 4.4, it was illustrated that a slightly activated other mode affects NES performance in dissipating the strongly activate mode. Now, we consider the case where both modes are significantly activated. The $a_1 - b_1$ and $a_2 - b_2$ sections of the SIM under strongly activated other modes for hardening stiffness are presented in Fig. 6a and b for modes 1 and 2, respectively. On the $a_1 - b_1$ section, the tongue protruding from the right branch eventually connects to the origin for increasing a_2. A new suboptimal left branch appears that, for a large range of a_1 (0–4.5), has a small b_1, deteriorating the NES performance for suppressing vibrations of the first mode. Regarding the $a_2 - b_2$ section, strongly activating a_1 not only makes part of the left branch unstable but also pushes the fold downwards. As such, the vibration threshold for a_2 decreases significantly, improving the energy dissipation properties on the second mode for a wide range of a_2. The SIM's sections for the softening stiffness, shown in Figs. 6c and d, exhibit the opposite effect. The local maximum of the $a_1 - b_1$ SIM section is pushed down with increasing a_2, which facilitates effective dissipation of the first mode's vibration energy. Conversely, a new suboptimal branch is generated in the $a_2 - b_2$ SIM section for increasing a_1, which deteriorates the dissipation performance of the second mode. In the next section, time series obtained from direct simulations are projected on the SIM to validate the relevance of its shape with respect to the system dynamics and NES performance.

4.5.2 Time simulation with constant modes

To validate the SIMs and the conclusions drawn from them, Eq. (30) is integrated in time with an ODE solver. To facilitate the comparison, one mode of the primary system is artificially kept constant by imposing the right-hand side of the first or the second equation of (30) equal to zero. Although this is a mathematical artifact, it enables us to validate the observations on the SIMs provided so far.

Results regarding both hardening and softening NES are provided in Fig. 7. Figure 7a–d refers to the case of a_2 constant, while Fig. 7e–h to a_1 constant. a_h is obtained from q_h as $a_h = \sqrt{q_h^2 + \dot{q}_h/\omega_h}$ and b_h from z by applying band-pass filters to filter once around ω_1 and once around ω_2. Then $b_h = \sqrt{z_h^2 + \dot{z_h}/\omega_h}$ where z_h is a filtered version of z around ω_h. The filtering causes unavoidable quantitative errors, which do not alter the qualitative dynamical scenario.

As discussed before regarding the hardening stiffness, for $a_2 > 0$, a new suboptimal branch is generated in the $a_1 - b_1$ SIM section, as illustrated in Fig. 7a. For $a_2 = 0$, modal amplitudes extracted from the corresponding numerical simulation for $a_1(0) = 3$ are depicted on the SIM in a dotted black line, and for $a_2 = 0.2$ in a dotted orange line. The corresponding time evolution of a_1 and b_1 is plotted in Fig. 7c and d with their corresponding colors. For $a_2 = 0$, the system dynamics is attracted to the right branch of the $a_1 - b_1$ SIM section, and the time evolution of a_1 shows that the dissipation of this modal energy takes approximately 1500 time units. At the same time, b_1 is nearly constant until a sudden drop at about $t = 1500$, after which the dynamics converges to the SIM's left branch, with a small b_1 amplitude. When $a_2 = 0.2$, the SIM is heavily distorted. The system converges to a SIM branch with very low b_1 values, resulting in very poor energy dissipation. Evolution of a_1 and b_1 in time (orange lines in Fig. 7c and d) confirms this observation. We note a significant quantitative mismatch between the SIM and the $a_1 - b_1$ trend observed from simulations (orange lines in Fig. 7a), which is probably caused by the presence of (sub)harmonics in the absorber vibrations; nevertheless, the qualitative behavior is still confirmed.

As already discussed, the softening stiffness causes an opposite effect, as illustrated by the SIM section in Fig. 7b. In the figure, the dotted yellow and purple lines correspond to time integrations obtained for $a_1(0) = 1$, where either $a_2 = 0$ (in yellow) or $a_2 = 0.4$ (in purple). The time evolutions of the modal amplitudes are shown in Fig. 7c and d with their corresponding colors. In this case, the suboptimal left branch of the SIM is pushed down by increasing a_2. For $a_2 = 0$, the numerical simulation shows a stagnant decay. The inset in Fig. 7b illustrates that the dynamics is attracted to the left suboptimal branch of the SIM; this occurs because $a_1(0) = 1$ is below the local maximum of the SIM. By increasing a_2 to 0.4, the left branch is pushed down and becomes partly unstable. Consequently, the system dynamics is attracted to the optimal right branch of the SIM, and the time evolution of a_1 shows a rapid decay; b_1 initially attains high amplitudes during the

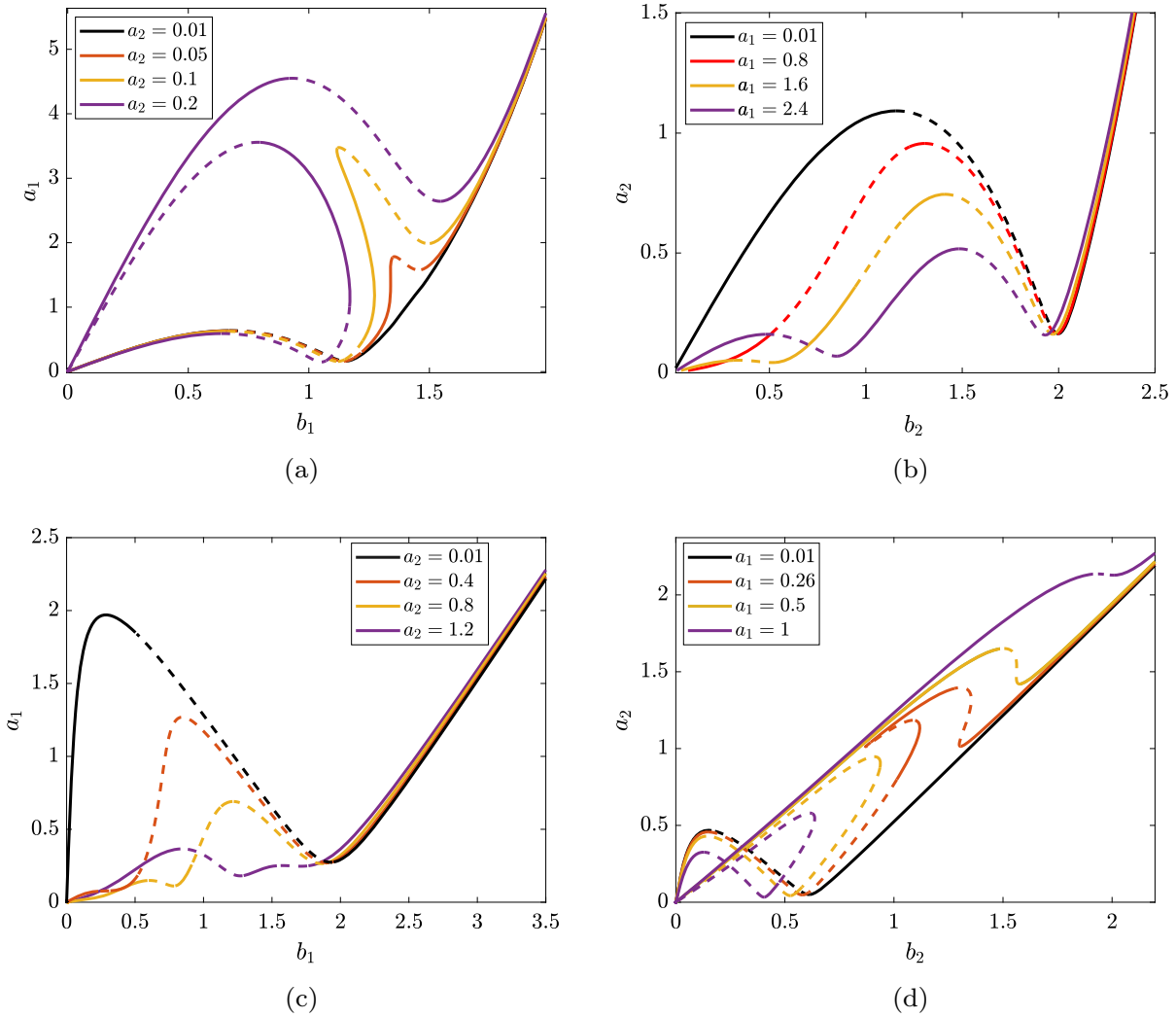

Fig. 6 Sections of the SIM for hardening **a**,**b** and softening **c**, **d** NES, to study the effect of strongly activated modes. **a** $a_1 - b_1$ SIM section for several constant a_2 (hardening NES); **b** $a_2 - b_2$ SIM section for several constant a_1 (hardening NES); **c** $a_1 - b_1$ SIM section for several constant a_2 (softening NES); **d** $a_2 - b_2$ SIM section for several constant a_1 (softening NES)

dissipation; then, its value drops as the system jumps to the left-most stable branch of the SIM.

We now study the effect of $a_1 \neq 0$ for energy dissipation of the second mode (a_2). The SIM sections for hardening stiffness are given in Fig. 7e. Modal amplitudes extracted from numerical simulations are superimposed to the SIM for the cases of $a_1 = 0$ (black dotted line) and $a_1 = 0.4$ (orange dotted line); initial conditions were set such that $a_2(0) = 0.8$. The time evolutions of the modal amplitudes a_2 and b_2 are depicted in Fig. 7g and h, respectively, with their corresponding colors. When $a_1 = 0$ (black lines), $a_2(0) = 0.8$ is below the SIM's local maximum, and the system dynamics converges to the suboptimal left branch, resulting in stagnant decay of a_2 and small b_2 values. Increasing a_1 ($a_1 = 0.4$), this branch becomes unstable, and the dynamics converges to the optimal right branch, with corresponding rapid decay of a_2 and high b_2 values. As soon as the local minimum of the SIM section in Fig. 7e is reached, the system dynamics jumps to the left branch, resulting in small b_2 values and a residual a_2.

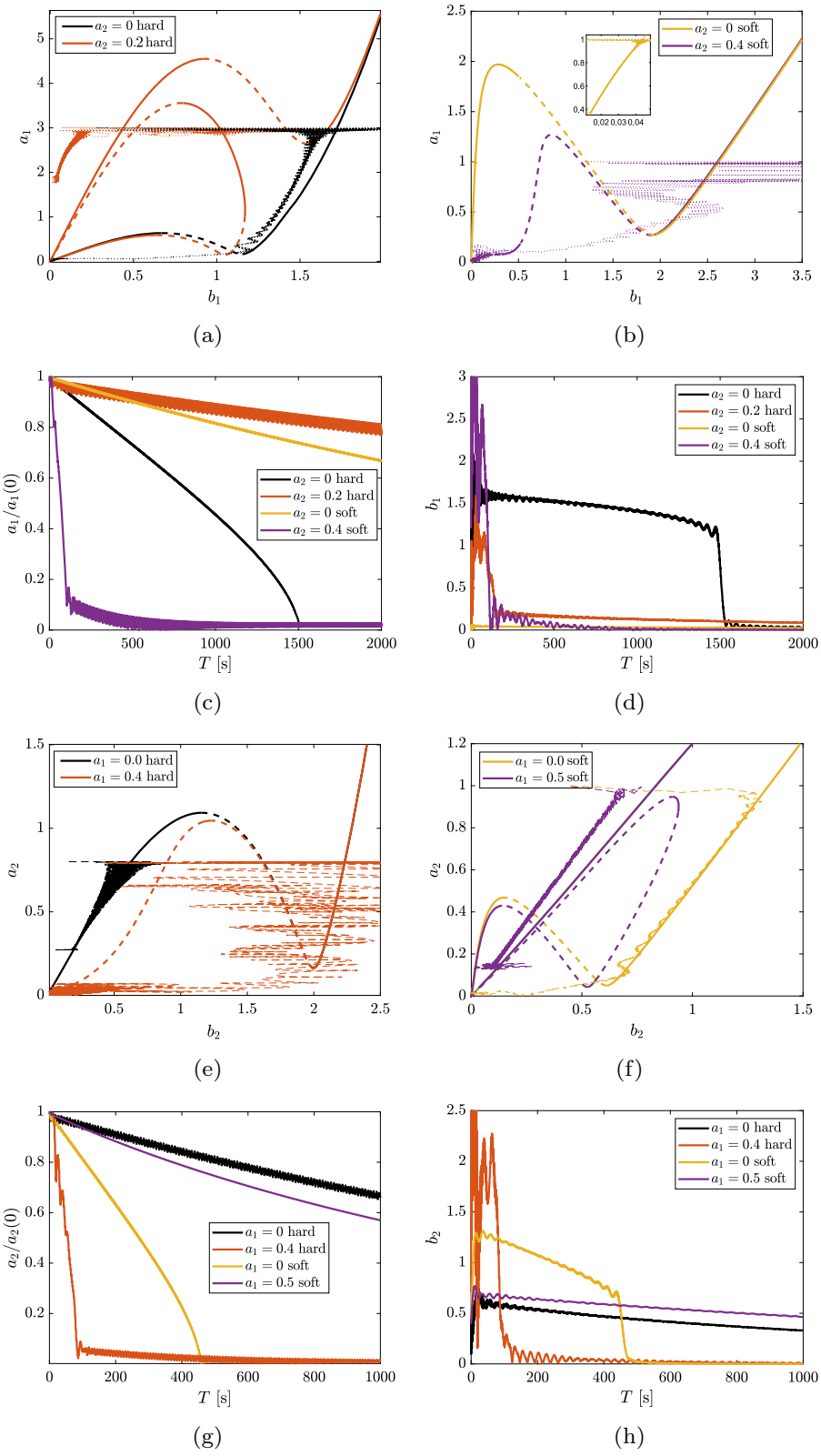

Fig. 7 Modal amplitudes extracted from numerical simulations of Eq. (30), overlapped to the analytically obtained SIM. **a**,**e** hardening NES, **b**, **f** softening NES; **a**–**d** a_2 artificially kept constant and a_1 decreasing in time, **e**)–**h** a_1 artificially kept constant and a_2 decreasing in time; **a**, **b**, **e**, **f** sections of the SIM, **c**, **d**, **g**, **h**) evolution in time of modal amplitudes. Initial conditions for the hardening case are $a_1(0) = 3$ and $a_2(0) = 0.8$, while for the softening case $a_1(0) = 1$ and $a_2(0) = 1$. In each case, either a_1 or a_2 is kept constant

Again the opposite happens for the softening stiffness. Figure 7f shows the SIM and modal amplitudes from numerical simulations for the cases of $a_1 = 0$ (yellow lines) and $a_1 = 0.5$ (purple lines); initial conditions are set such that $a_2(0) = 1$. The time evolution of the modal amplitudes is represented in Figs. 7g and 7h with their corresponding colors. For $a_1 = 0$, the system dynamics converges to the right branch of the SIM, while for $a_1 = 0.5$, it goes toward a new suboptimal branch created from the fold of the modal interaction. Accordingly, Fig. 7g and h shows a fast decay for $a_1 = 0$ and slow decay for $a_1 = 0.5$.

To sum up the analysis performed in this section, our investigation reveals that for a hardening NES, a small amount of energy on the higher frequency mode is sufficient to degrade the dissipation performance of the lower frequency mode. On the other hand, vibration energy on the lower frequency mode does not negatively affect the energy dissipation of the higher frequency mode. In contrast, the opposite is true for a softening NES. In some sense, a hardening NES appears to prioritize energy dissipation of the higher frequency mode, while a softening NES prioritizes the energy dissipation of the lower frequency mode. In the next section, the complete system is simulated, and both modes will be able to interact and decay concurrently, which enables the triggering of the resonance capture cascade phenomenon.

5 (Inverted) resonance capture cascade

The full dynamical system in Eq. (28) is now simulated with both modes initially equally activated in terms of kinetic energy, i.e., $a_1(0) = 1$ and $a_2(0) = 1/\sqrt{3}$.

5.1 Hardening stiffness: RCC

At first, we consider the hardening NES. The result of the simulation is shown in Fig. 8. The vibrations of the physical coordinates x_1 and z are shown in Figs. 8a and b. First high-frequency vibrations of the primary system decay and then low-frequency vibrations. The wavelet transformation of the NES relative displacement z illustrates that the NES engages sequentially with the vibration modes, from high to low frequency, the transition being at about $t = 90$. This phenomenon is called RCC and is well known to occur for the conventional hardening cubic-stiffness NES. RCC is even more clearly recognizable looking at the modal vibration content of the primary system, depicted in Figs. 8d and e, where first only the second mode (a_2) decays. At about $t = 90$, the first mode (a_1) engages in the cascade and start decaying. The modes in the NES show a high, near-constant amplitude in the second mode (b_2) before switching to the first one (b_1). The time evolution of the modal amplitudes is projected on the SIM sections $a_1 - b_1$ and $a_2 - b_2$ in Figs. 8f and g. On the $a_1 - b_1$ section, the numerical simulation (dotted orange line) first sits on the black SIM, where $a_2 = 1$. Only once a_2 is sufficiently decayed, the dynamics converges to the optimal right branch of the yellow SIM. On the $a_2 - b_2$ section, the system dynamics immediately converges to the optimal right branch. Once the branch is descended, the numerical simulations are attracted to the left branch.

In order to have a more comprehensive illustration of the RCC and its connection to the SIM, a 3-dimensional representation of the SIM is provided in Figs. 8h (a_1, a_2, b_1) and 8i (a_1, a_2, b_2); in the figures, the modal amplitudes collected from the numerical simulation are overlapped to the SIM. The curves clearly show how the SIM provides a consistent qualitative description of the system dynamics.

5.2 Softening stiffness: IRCC

We now consider the case of a softening NES through a numerical simulation, whose results are provided in Fig. 9. The vibrations of the physical coordinates x_1 and z (Fig. 9a and b) show an opposite picture compared to a hardening stiffness NES. The NES vibrates first with the lower frequency mode and then the higher frequency mode, which can be better seen in the wavelet transform of the NES of Fig. 9c. Accordingly, in the host system, the lower frequency mode is dissipated first. The same is observed in modal coordinates (Fig. 9d and e), where first a_1 decays and b_1 is large. Only once a_1 is sufficiently small, a_2 decays as well, thanks to increased b_2 values. The SIMs and numerical simulations in Fig. 9f and g show good qualitative agreement; we note that the dynamics is first attracted to the right branch of the $a_1 - b_1$ SIM section (Fig. 9f) and to the left branch of the $a_2 - b_2$ section (Fig. 9g). Once the local minimum of the SIM is reached, the system dynamics jumps to the other

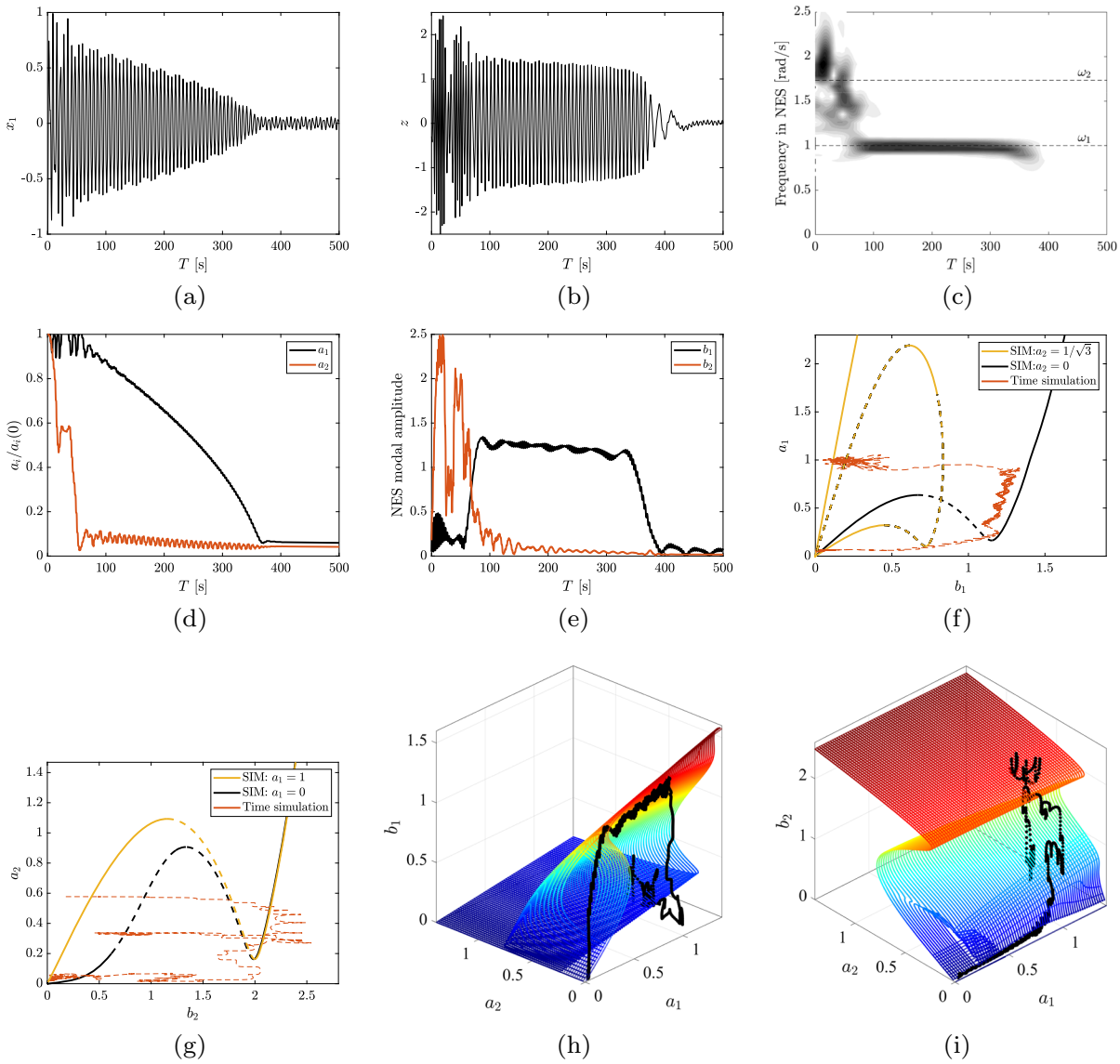

Fig. 8 Time simulation of (28) where $f_{\text{nl}} = \varepsilon z^3$ is the hardening NES stiffness, initial conditions such that $a_1(0) = 1$ and $a_2(0) = 1/\omega_2$. **a** first mass displacement x_1; **b** absorber relative displacement z; **c** absorber relative displacement wavelet transform; **d** primary system's modal amplitudes a_1 and a_2; **e** NES's modal amplitude b_1 and b_2; **f** $a_1 - b_1$ SIM sections with overlapped modal amplitudes varying in time; **g** $a_2 - b_2$ SIM section with overlapped modal amplitudes varying in time; **h**, **i** 3-dimensional SIM representations with overlapped modal amplitudes varying in time

branch. A more comprehensive view of the comparison between the SIM and the simulated dynamics is provided by the 3-dimensional representation of the SIM in Figs. 9h and i. Considering the main character of the dynamical phenomenon just described, i.e., that the NES first interacts with low-frequency modes, and then with high-frequency modes, this kind of motion is named inverted resonance capture cascade. Observe that the performance of both the softening and hardening NES is in the some order, the hardening NES dissipates the energy over about 370 time units, while the softening NES takes 310 time units. Finally, in Fig. 9c, an increasing frequency in the NES is observed after the RCC. This is because the NES loses synchronization

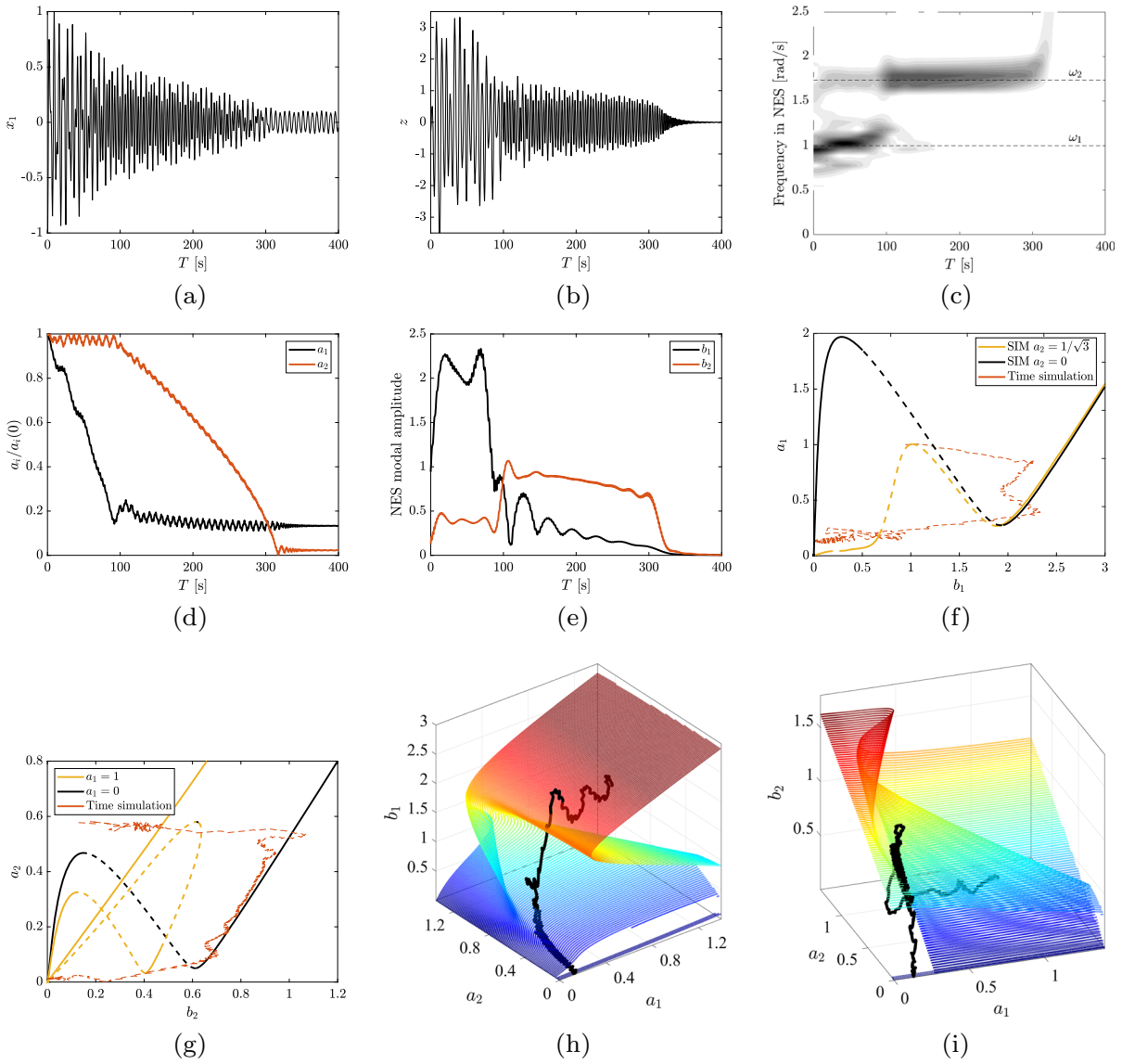

Fig. 9 Time simulation of (28) where $f_{\text{nl}} = \varepsilon \arctan(20z)$ is the softening NES stiffness, initial conditions such that $a_1(0) = 1$ and $a_2(0) = 1/\omega_2$. **a** first mass displacement x_1; **b** absorber relative displacement z; **c** absorber relative displacement wavelet transform; **d** primary system's modal amplitudes a_1 and a_2; **e** NES's modal amplitude b_1 and b_2; **f** $a_1 - b_1$ SIM sections with overlapped modal amplitudes varying in time; **g** $a_2 - b_2$ SIM section with overlapped modal amplitudes varying in time; **h**, **i** 3-dimensional SIM representations with overlapped modal amplitudes varying in time

with the modal frequencies of the host system at lower amplitudes. At these amplitudes, the NES reverts to its own natural frequency, which increases for decreasing amplitudes as seen in Sect. 2. For the cubic hardening NES, the frequency in the NES decreases after RCC, as it loses synchronization with the modes and jumps to a lower backbone of nonlinear mode, which has a decreasing frequency [26].

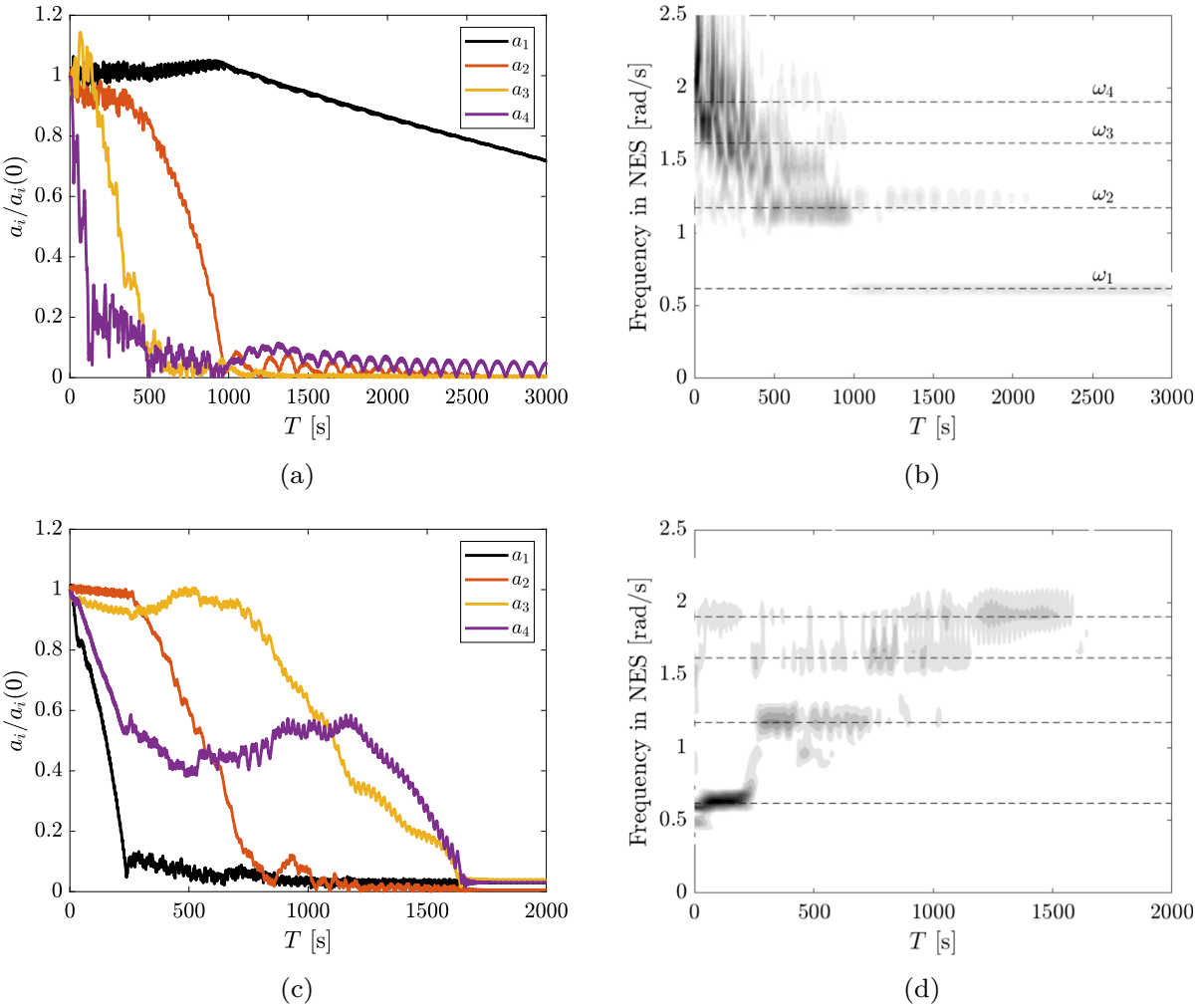

Fig. 10 Evolution of the modal amplitudes in time, for the four-DOF chain of masses, with an attached NES. **a**, **b** hardening NES, **c**, **d** softening NES. **a**, **c** evolution in time of the host system's modal amplitudes, **b**, **d** wavelet transformation of the NES relative displacement

5.3 Four-DOF system

In order to further validate the existence and engineering relevance of the IRCC, we now consider a four-DOF host system. The system consists of an undamped chain of four unit masses attached to each other through identical unit springs; its dimensionless natural frequencies are 0.618, 1.1756, 1.618 and 1.9021. The NES is attached to the second mass. In practice, the system is an extension of the one shown in Fig. 2. First, we consider the case of a hardening NES, then a softening one. The system is studied solely through numerical simulations to validate the existence of the IRCC. The results of the numerical simulations are illustrated in Fig. 10. Figure 10a and b refers to the hardening NES, while Fig. 10c and d to the softening NES. In the figures, the decay in time of the host system's modal amplitudes and the wavelet transformation of the NES relative displacement are illustrated for the two cases, respectively.

Referring to the hardening case, we observe (Fig. 10a) how, initially, modal amplitude a_4 rapidly decreases, while a_1, a_2 and a_3 do not decrease at all—they actually slightly increase, as also observed in [29]. As proved by the wavelet transformation in Fig. 10b, at the same time, the NES is tuned to the fourth mode. Once a_4 reaches a small enough value, the NES starts

oscillating according to the third mode, and simultaneously a_3 rapidly decreases. After that, when also a_3 has a small enough value, the NES tunes to the second mode, and the second vibration mode of the host system (a_2) is dissipated. Finally, the NES tunes to the first mode, completing the RCC. The higher the mode, the faster the dissipation because of the higher frequency involved.

We now consider the softening NES. Looking at the evolution of the modal amplitudes in time (Fig. 10c), the expected IRCC can be recognized. Namely, first a_1 decays, then a_2, after that a_3 and finally a_4. The mechanisms are analogous to the one observed for the hardening case but with an inverted order. The inverted cascade is even more evident from the wavelet transformation of the NES relative displacement (Fig. 10d). The NES vibrates according to the four modes of the primary system, from the first to the fourth one. The wavelet transformation shows that, initially, the NES vibrates also according to the fourth mode, although with a relatively small intensity, which causes a partial dissipation of the fourth mode concurrently to the first one. This effect is not part of the IRCC and is probably due to modal interactions, which are hard to predict but often present. Indeed, the larger the number of activated modes of the primary system, the more modal interactions are developed, even if the natural frequencies have irrational ratios. Modal interactions can be identified from the wavelet transformation of the NES relative displacement, both for the hardening and the softening cases (Fig. 10b and d). This phenomenon was also observed in [29]. To predict them analytically, modal interactions should be considered while obtaining the SIM. However, this significantly complicates its derivation and enlarges its dimension. It is, therefore, out of the scope of this study.

Regarding the performance of the NESs, while it was similar in the two-DOF case for the softening and hardening NES, here the softening NES is clearly superior, as it is better in dissipating the slower modes. The softening NES is able to dissipate all modes in just over 1600 time units, while in the hardening case, the host system still contains a significant amount of energy in the first mode even after 3000 time units. However, since neither NES was optimized, any comparison of their performance is limited in scope.

To verify the generality of the phenomenon, simulations of the system with an attached softening NES, having the restoring force function $\mathrm{sgn}\,(x_\mathrm{a})\,\sqrt[3]{|x_\mathrm{a}|}$ (see Sect. 2), were also performed. However, they did not exhibit any qualitative difference from the NES with a saturating restoring force considered in the rest of the paper. Therefore, the corresponding figure is omitted for the sake of brevity.

In summary, our analysis confirms that a hardening NES triggers an RRC, dissipating energy one-by-one from the highest to the lowest frequency mode, and reveals that a softening NES leads to an IRCC, where energy is dissipated from the lowest to the highest frequency mode.

6 Conclusions

This study unveiled the existence of the so-called inverted resonance capture cascade (IRCC), which indicates the subsequent engagement of an NES with the vibration modes of the host system, starting from the lowest frequency to the highest one. This phenomenon is opposite to the well-known RCC, where the NES engages first with the highest frequency mode and last with the lowest frequency one. The transition from the classical RCC to the IRCC is related to adopting a softening stiffness characteristic of the NES instead of a hardening one. The performed analysis exploits multi-dimensional SIMs obtained by combining harmonic balance with a multiple-scale technique. By comparing modal amplitudes extracted from numerical simulations, the relevance of the SIM to the system dynamics was validated considering a two-DOF primary system; the SIM enabled us to explain the dynamical phenomena involved. The IRCC was also illustrated for a four-DOF primary system.

From an engineering perspective, the IRCC provides several benefits with respect to the classical RCC. The main one is that low-frequency modes are usually the most dangerous from a structural point of view since they cause larger displacements than higher frequency modes. Thus, their quicker dissipation is an important benefit.

Several aspects were overlooked in this study, which should be further investigated. In particular, we noted that modal interactions and combinatorial resonances have an important role in the NES dynamics, which was not analyzed. However, observing the frequency content of NES from the simulations, these resonances do not seem to qualitatively affect the IRCC, as also observed in [29]. A more involved analytical approach

is required for their analysis, which is out of the scope of this paper.

The practical realization of a softening NES poses specific challenges. Although previous studies addressed the realization of NESs with almost arbitrary stiffness forces [30,36,44–49], they were never utilized for real engineering applications, but only for academic studies; therefore, potential technical limitation might arise for their industrial exploitation.

In the present study, the IRCC was investigated from a purely phenomenological perspective, and no attempt to optimize its performance was made. Optimization is an important aspect that should be evaluated for assessing the real benefit of a softening NES. The optimization should also consider various shapes of the restoring force function. This is an essential step for comparing the performance of hardening and softening NESs.

Funding Open access funding provided by Budapest University of Technology and Economics. Giuseppe Habib acknowledges the financial support of the National Research, Development and Innovation Fund (Grant no. BME-NVA-02 and TKP2021-EGA-02) provided by the Ministry of Innovation and Technology financed under the TKP2021 funding scheme and by the National Research, Development and Innovation Office (Grant no. NKFI-134496).

Data availability Not applicable.

Declarations

Conflict of interest The authors declare that they have no conflict of interest.

Code availability The data and the code utilized for generating the presented results are available from the authors upon request.

References

1. Manevitch, L.I., Musienko, A.I., Lamarque, C.H.: New analytical approach to energy pumping problem in strongly nonhomogeneous 2dof systems. Meccanica **42**, 77–83 (2007)
2. Vakakis, A.F., Gendelman, O.V., Bergman, L.A., McFarland, D.M., Kerschen, G., Lee, Y.S.: Nonlinear Targeted Energy Transfer in Mechanical and Structural Systems, vol. 156. Springer Science Business Media, New York (2008)
3. Gendelman, O., Starosvetsky, Y., Feldman, M.: Attractors of harmonically forced linear oscillator with attached nonlinear energy sink i: description of response regimes. Nonlinear Dyn. **51**(1), 31–46 (2008)
4. Den Hartog, J.P.: Mechanical Vibrations. Courier Corporation, Chelmsford (1985)
5. Gendelman, O.: Analytic treatment of a system with a vibro-impact nonlinear energy sink. J. Sound Vib. **331**(21), 4599–4608 (2012)
6. Gourc, E., Seguy, S., Michon, G., Berlioz, A., Mann, B.: Quenching chatter instability in turning process with a vibro-impact nonlinear energy sink. J. Sound Vib. **355**, 392–406 (2015)
7. Farid, M., Gendelman, O., Babitsky, V.: Dynamics of a hybrid vibro-impact nonlinear energy sink. ZAMM-J. Appl. Math. Mech. Zeitschr. Angew. Math. und Mech. **101**(7), e201800341 (2021)
8. AL-Shudeifat, M.A., Wierschem, N.E., Bergman, L.A., Vakakis, A.F.: Numerical and experimental investigations of a rotating nonlinear energy sink. Meccanica **52**(4), 763–779 (2017)
9. Saeed, A.S., AL-Shudeifat, M.A., Vakakis, A.F.: Rotary-oscillatory nonlinear energy sink of robust performance. Int. J. Non-Linear Mech. **117**, 103–249 (2019)
10. Romeo, F., Sigalov, G., Bergman, L.A., Vakakis, A.F.: Dynamics of a linear oscillator coupled to a Bistable light attachment: numerical study. J. Comput. Nonlinear Dyn. (2015). https://doi.org/10.1115/1.4027224
11. Habib, G., Romeo, F.: The tuned bistable nonlinear energy sink. Nonlinear Dyn. **89**(1), 179–196 (2017)
12. Al-Shudeifat, M.A., Saeed, A.S.: Frequency-energy plot and targeted energy transfer analysis of coupled bistable nonlinear energy sink with linear oscillator. Nonlinear Dyn. **105**(4), 2877–2898 (2021)
13. Vakakis, A.F.: Shock isolation through the use of nonlinear energy sinks. J. Vib. Control **9**(1–2), 79–93 (2003)
14. Vakakis, A.F., Gendelman, O.V., Bergman, L.A., Mojahed, A., Gzal, M.: Nonlinear targeted energy transfer: state of the art and new perspectives. Nonlinear Dyn. **108**(2), 711–741 (2022)
15. Starosvetsky, Y., Gendelman, O.: Attractors of harmonically forced linear oscillator with attached nonlinear energy sink. II: optimization of a nonlinear vibration absorber. Nonlinear Dyn. **51**(1), 47–57 (2008)
16. Hubbard, S.A., McFarland, D.M., Bergman, L.A., Vakakis, A.F.: Targeted energy transfer between a model flexible wing and nonlinear energy sink. J. Aircr. **47**(6), 1918–1931 (2010)
17. Zulli, D., Luongo, A.: Nonlinear energy sink to control vibrations of an internally nonresonant elastic string. Meccanica **50**(3), 781–794 (2015)

18. Ture Savadkoohi, A., Lamarque, C.H., Weiss, M., Vaurigaud, B., Charlemagne, S.: Analysis of the 1: 1 resonant energy exchanges between coupled oscillators with rheologies. Nonlinear Dyn. **86**, 2145–2159 (2016)
19. Lee, Y.S., Vakakis, A.F., Bergman, L.A., McFarland, D.M., Kerschen, G.: Enhancing the robustness of aeroelastic instability suppression using multi-degree-of-freedom nonlinear energy sinks. AIAA J. **46**(6), 1371–1394 (2008)
20. Bergeot, B., Bellizzi, S., Berger, S.: Dynamic behavior analysis of a mechanical system with two unstable modes coupled to a single nonlinear energy sink. Commun. Nonlinear Sci. Numer. Simul. **95**, 105623 (2021)
21. Bichiou, Y., Hajj, M.R., Nayfeh, A.H.: Effectiveness of a nonlinear energy sink in the control of an aeroelastic system. Nonlinear Dyn. **86**(4), 2161–2177 (2016)
22. Habib, G., Kerschen, G.: Suppression of limit cycle oscillations using the nonlinear tuned vibration absorber. Proc. Royal Soc. A: Math., Phys. Eng. Sci. **471**(2176), 20140976 (2015)
23. Luongo, A., Zulli, D.: Dynamic analysis of externally excited NES-controlled systems via a mixed multiple scale/harmonic balance algorithm. Nonlinear Dyn. **70**, 2049–2061 (2012)
24. Vakakis, A.F., Manevitch, L., Gendelman, O., Bergman, L.: Dynamics of linear discrete systems connected to local, essentially non-linear attachments. J. Sound Vib. **264**(3), 559–577 (2003)
25. Vakakis, A.F., McFarland, D.M., Bergman, L., Manevitch, L.I., Gendelman, O.: Isolated resonance captures and resonance capture cascades leading to single-or multi-mode passive energy pumping in damped coupled oscillators. J. Vib. Acoust. **126**(2), 235–244 (2004)
26. Kerschen, G., Kowtko, J.J., McFarland, D.M., Bergman, L.A., Vakakis, A.F.: Theoretical and experimental study of multimodal targeted energy transfer in a system of coupled oscillators. Nonlinear Dyn. **47**(1), 285–309 (2007)
27. Kerschen, G., Lee, Y.S., Vakakis, A.F., McFarland, D.M., Bergman, L.A.: Irreversible passive energy transfer in coupled oscillators with essential nonlinearity. SIAM J. Appl. Math. **66**(2), 648–679 (2005)
28. Dekemele, K., De Keyser, R., Loccufier, M.: Performance measures for targeted energy transfer and resonance capture cascading in nonlinear energy sinks. Nonlinear Dyn. **93**(2), 259–284 (2018)
29. Habib, G., Romeo, F.: Tracking modal interactions in nonlinear energy sink dynamics via high-dimensional invariant manifold. Nonlinear Dyn. **103**(4), 3187–3208 (2021)
30. Dekemele, K., Van Torre, P., Loccufier, M.: Design, construction and experimental performance of a nonlinear energy sink in mitigating multi-modal vibrations. J. Sound Vib. **473**, 115243 (2020)
31. Kovacic, I., Brennan, M.J.: The Duffing Equation: Nonlinear Oscillators and their Behaviour. Wiley, Hoboken (2011)
32. McFarland, D.M., Kerschen, G., Kowtko, J.J., Lee, Y.S., Bergman, L.A., Vakakis, A.F.: Experimental investigation of targeted energy transfers in strongly and nonlinearly coupled oscillators. J. Acoust. Soc. Am. **118**(2), 791–799 (2005)
33. Ture Savadkoohi, A., Vaurigaud, B., Lamarque, C.H., Pernot, S.: Targeted energy transfer with parallel nonlinear energy sinks, part II: theory and experiments. Nonlinear Dyn. **67**(1), 37–46 (2012)
34. Lamarque, C.H., Savadkoohi, A.T., Charlemagne, S.: Experimental results on the vibratory energy exchanges between a linear system and a chain of nonlinear oscillators. J. Sound Vib. **437**, 97–109 (2018)
35. Zeng, Y.C., Ding, H., Du, R.H., Chen, L.Q.: Micro-amplitude vibration suppression of a bistable nonlinear energy sink constructed by a buckling beam. Nonlinear Dyn. **108**, 1–23 (2022)
36. Lo Feudo, S., Touzé, C., Boisson, J., Cumunel, G.: Nonlinear magnetic vibration absorber for passive control of a multistorey structure. J. Sound Vib. **438**, 33–53 (2019)
37. Benacchio, S., Malher, A., Boisson, J., Touzé, C.: Design of a magnetic vibration absorber with tunable stiffnesses. Nonlinear Dyn. **85**(2), 893–911 (2016)
38. Chen, Y., Zhao, W., Shen, C., Qian, Z.: Bistable nonlinear energy sink using magnets and linear springs: application to structural seismic control. Shock Vib **2021**, 1–17 (2021)
39. Yao, H., Cao, Y., Zhang, S., Wen, B.: A novel energy sink with piecewise linear stiffness. Nonlinear Dyn. **94**(3), 2265–2275 (2018)
40. Farid, M., Gendelman, O.V.: Tuned pendulum as nonlinear energy sink for broad energy range. J. Vib. Control **23**(3), 373–388 (2017)
41. Dekemele, K., Habib, G., Loccufier, M.: The periodically extended stiffness nonlinear energy sink. Mech. Syst. Signal Process. **169**, 108706 (2022)
42. Weiss, M., Chenia, M., Ture Savadkoohi, A., Lamarque, C.H., Vaurigaud, B., Hammouda, A.: Multi-scale energy exchanges between an elasto-plastic oscillator and a light nonsmooth system with external pre-stress. Nonlinear Dyn. **83**, 109–135 (2016)
43. Chen, J.E., Sun, M., Hu, W.H., Zhang, J.H., Wei, Z.C.: Performance of non-smooth nonlinear energy sink with descending stiffness. Nonlinear Dyn. **100**, 1–13 (2020)
44. Zou, D., Liu, G., Rao, Z., Tan, T., Zhang, W., Liao, W.H.: A device capable of customizing nonlinear forces for vibration energy harvesting, vibration isolation, and nonlinear energy sink. Mech. Syst. Signal Process. **147**, 107101 (2021)
45. Zou, D., Chen, K., Rao, Z., Cao, J., Liao, W.H.: Design of a quad-stable piezoelectric energy harvester capable of programming the coordinates of equilibrium points. Nonlinear Dyn. **108**, 1–15 (2022)
46. Dou, S., Strachan, B.S., Shaw, S.W., Jensen, J.S.: Structural optimization for nonlinear dynamic response. Philos. Trans. Royal Soc. A: Math., Phys. Eng. Sci. **373**(2051), 20140408 (2015)
47. Dou, S., Jensen, J.S.: Optimization of hardening/softening behavior of plane frame structures using nonlinear normal modes. Comput. Struct. **164**, 63–74 (2016)
48. Tao, H., Danzi, F., Silva, C.E., Gibert, J.M.: Heterogeneous digital stiffness programming. Extrem. Mech. Lett. **55**, 101832 (2022)
49. Habib, G., Grappasonni, C., Kerschen, G.: Passive linearization of nonlinear resonances. J. Appl. Phys. **120**(4), 044901 (2016)
50. Urabe, M.: Galerkin's procedure for nonlinear periodic systems. Arch. Ration. Mech. Anal. **20**(2), 120–152 (1965)
51. Karkar, S., Cochelin, B., Vergez, C.: A comparative study of the harmonic balance method and the orthogonal collocation method on stiff nonlinear systems. J. Sound Vib. **333**(12), 2554–2567 (2014)

52. Krack, M., Gross, J.: Harmonic Balance for Nonlinear Vibration Problems, vol. 1. Springer, Cham (2019)
53. Manevitch, L.: The description of localized normal modes in a chain of nonlinear coupled oscillators using complex variables. Nonlinear Dyn. **25**, 95–109 (2001)
54. Guskov, M., Thouverez, F.: Harmonic balance-based approach for quasi-periodic motions and stability analysis. J. Vib. Acoust. **134**(3), 031003 (2012)
55. Ju, R., Fan, W., Zhu, W., Huang, J.: A modified two-timescale incremental harmonic balance method for steady-state quasi-periodic responses of nonlinear systems. J. Comput. Nonlinear Dyn. **12**(5), 051007 (2017)
56. Dekemele, K., Van Torre, P., Loccufier, M.: Performance and tuning of a chaotic bi-stable NES to mitigate transient vibrations. Nonlinear Dyn. **98**(3), 1831–1851 (2019)
57. Petit, F.: Exploring the limitations of linear and nonlinear vibration absorbers. Ph.D. thesis, Ghent University (2012)